2023-12-01

# Characterization Of Developmental Phenotypes In Zebrafish With Mutations In Mmachc

Briana Elise Pinales
*University of Texas at El Paso*

CHARACTERIZATION OF DEVELOPMENTAL PHENOTYPES IN ZEBRAFISH WITH MUTATIONS IN *MMACHC*

BRIANA E. PINALES

Doctoral Program in Biological Sciences

APPROVED:

Anita M. Quintana, Ph.D., Chair

Charles Spencer, Ph.D.

Katherine Serafine, Ph.D.

Siddhartha Das, Ph.D

German Rosas-Acosta, Ph.D.

Stephen L. Crites, Jr., Ph.D.

Dean of the Graduate School

## Dedication

Dedicated to my brother David, who lives with Ehlers Danlos syndrome, a rare condition that affects the connective tissue causing the common phenotype of joint hypermobility. I've been fortunate to be able to concentrate on a branch of science that most people overlook. I hope that my dissertation can console others by knowing there are individuals researching rare genetic diseases, that these patients are not alone, and there are scientists that are invested in helping. My brother had a few mild symptoms when we were younger, but he wasn't diagnosed until he was in his early twenties. Despite the enthusiasm of the many physicians he visited, none of the doctors knew how to properly evaluate him. Unfortunately, we received more questions than answers. He was later diagnosed with Munchausen syndrome by proxy- as it is a safe and easy diagnostic solution for physicians who lack the clinical experience. Nonetheless, I would like to dedicate this to my brother David. It only takes one person to pave the path towards making a difference and with time those changes will come to fruition. I love you.

# CHARACTERIZATION OF DEVELOPMENTAL PHENOTYPES IN ZEBRAFISH WITH MUTATIONS IN *MMACHC*

by

BRIANA E. PINALES, B.S.

DISSERTATION

Presented to the Faculty of the Graduate School of Biosciences

The University of Texas at El Paso

in Partial Fulfillment

of the Requirements

for the Degree of

DOCTOR OF PHILOSOPHY

Department of Biological Sciences

THE UNIVERSITY OF TEXAS AT EL PASO

December 2023

**Acknowledgements**

To everyone that has helped me over the years; thank you for being there when I needed it the most. I would also like to acknowledge my SPINES family (2017), my Neurobiology family (2018), and my UTEP family, for all the love and laughs. A special thanks to all my mentees who were there when I needed it the most. A special thanks to my committee; Time is more precious than money, and for that, I thank you!

I would like to acknowledge and thank my mentor, Dr. Anita M. Quintana. You took an eccentric person like me into your lab, gave me a set of pipettes, a bench beside you, creative freedom, and with mutual efforts, we produced great science! Thank you for all the mentorship, patience, and support. Undeniably, I could not have made this major milestone without you.

Finally, I would like to thank my family and friends. Specifically, my grandparents, parents, brothers (David and Baby), sister (Ari), my Tia yaya, Uncle Shaun, Shaunie and Victoria. Thank you for bringing baby Wesley in your place, uncle Shaun. To Alex, you loved to make me mad; moreso that you left earth so soon and left me here to miss you. To my grandparents, who have sacrificed so much for my happiness. You would give me your branches, apples, leaves, and trunk to see me happy. I would not be able to do anything without your love and support. Lastly, I would like to acknowledge my mom. I do everything for you and because of you. I love you.

## Table of Contents

## List of Tables

## List of Figures

## Chapter 1. Introduction

*"Although rare diseases each affect a small number of people, taken together, they affect millions. Better diagnosis and understanding of the underlying mechanisms are needed. By combining phenotypic data for many rare disease patients, comorbidity patterns, along with their underlying molecular systems, can give important insights into disease mechanisms, moreover they can be used to direct differential-diagnosis of rare disease patients."*

*-Diaz-Santiago et al. 2020.*

Rare genetic diseases are seldom a priority in research, partly due to the low prevalence in the population. While cases are individually rare, collectively, the 'rare' qualities are ascribed to more than 7000 distinct disorders (Marwaha et al., 2022). About 30 million people, or 1 in 10, are affected by these diseases, making them collectively as prevalent as type 2 diabetes (Marwaha et al., 2022). The misconception that they are "rare" hinders the understanding of basic mechanisms, preventative measures, effective diagnostic testing, and, ultimately, therapeutic development. The average time a patient will spend finding an accurate diagnosis is around 4-5 years, and in some cases, it can take as long as a decade.

The stark reality is that those affected by such anomalies will spend their lifetime undiagnosed, misdiagnosed, or on an endless diagnostic journey (Marwaha et al., 2022). Therefore, studying anomalies in early development provides insight into fundamental mechanisms that can be applied to more common diseases. This study is focused on inborn errors of vitamin B12 metabolism. The occurrence of these metabolic abnormalities is rare and may significantly impact the growth and development of the fetus; because of this, individuals may place varying

levels of urgency on the study of congenital disabilities. If all individuals were to possess comparable experiences, the majority would likely acknowledge the fundamental significance of this research. The impact on the family is indeed disheartening. Consequently, it is important to emphasize the importance of this information in elucidating the necessity for additional fundamental scientific research in the subsequent chapters.

## INBORN ERRORS OF METABOLISM

Inborn errors of metabolism (IEMs) are a collection of inherited diseases that arise from disruptions in metabolic pathways due to impaired enzymatic activity (Lee & Kim, 2022; Van De Burgt et al., 2023). The disruption can arise due to a deficiency in certain enzymes within the human cell, resulting in the cell's inability to carry out essential biochemical processes. Often, IEMs can present themselves during early childhood or diagnosed with newborn screening (NBS). However, the sensitivity of the panels used with NBS to identify IEMs varies widely, and some of these diseases manifest into adolescence or adulthood without previous symptoms in childhood (Van De Burgt et al., 2023).

### *cblC* syndrome

Methylmalonic aciduria and homocystinuria, cblC type (*cblC*) syndrome (MIM 277400) is one of the most common inborn errors of vitamin B12 (cobalamin) metabolism (Agarwal et al., 2021; Beauchamp et al., 2009; Frattini et al., 2010; Nguyen et al., 2022; Rosenblatt et al., 1997; Weisfeld-Adams et al., 2013). It is known for its heterogeneous nature that causes multisystemic damage. *cblC* syndrome is an autosomal recessive disorder that results from pathogenic variants in the methylmalonic aciduria and homocystinuria type C (*MMACHC*) gene (Lee & Kim, 2022). Defective MMACHC protein impairs the conversion of cobalamin (Cbl) into its physiologically active forms, methylcobalamin (MeCbl) and adenosylcobalamin (AdoCbl). Without the active

forms of Cbl, there is a toxic accumulation of metabolites, consequently causing a disturbance in several biological processes. Most notably, c*blC* syndrome presents itself in two separate forms: early and late-onset. The latter being the easiest to treat.

***Early onset cblC syndrome***

In early onset *cblC* syndrome, the brain is severely affected, resulting in clinical presentations of poor feeding, dysmorphic features, microcephaly, encephalopathy, hypotonia, developmental delays, and seizures (Sloan et al., 2020). Neuroradiologic investigations have identified heterogeneity in brain abnormalities. For example, Rossi et al. (2001) reported neurodevelopmental deficits observed in 12 early onset cases, in which a patient was described to have a raised intracranial pressure and tetraventricular hydrocephalus. In contrast, in 2 other cases, delayed myelination was observed. In addition, Rossi et al. (2001) found that diffuse supratentorial white matter swelling with prominent hyperintensity on T2-weighted magnetic resonance images was the most common feature of the early untreated stages of the disease. The study mentions that there is evidence to suggest that S-adenosylmethionine, a methyl donor in the human brain, is strongly related to white matter demyelination (Rossi et al., 2001). Myelinopathy is a dominant pathologic feature in hyperhomocysteinemias, together with vascular abnormalities. If there is decreased activity of methionine synthase, there is a reduction in the availability of methionine for conversion to S-adenosylmethionine, possibly explaining the observed myelinopathy and subsequent white matter loss. A disruption in the activity of methylmalonyl-CoA mutase results in the accumulation of methylmalonyl-CoA and its precursor, propionylCoA (Rossi et al., 2001). Consequently, non-physiological fatty acids with an odd number of carbon atoms are synthesized and incorporated into neuronal lipids. Ultimately, the study found that the clinical presentations

were nonspecific, a primary reason why diagnosis relies on biochemical analysis (Rossi et al., 2001).

### *Late-onset cblC*

In late-onset *cblC* there is progressive cognitive decline, neuropsychiatric symptoms, and subacute combined spinal cord degeneration (Agarwal et al., 2021; Rosenblatt et al., 1997; Sloan et al., 2020). Patients with late-onset typically present after 4 years of age with milder forms of neurologic dysfunction (Rossi et al., 2001). However, no matter the age of the initial presentation, neurological symptoms differ greatly between early and late onset patients. According to Rosenblatt et al. (1997) neonates and infants experienced a generalized nonfocal neurological problems whereas the older children had issues in the spinal cord and extrapyramidal components of the motor system, intellectual function, and mental status (Rosenblatt et al., 1997). Older patients present predominantly neuropsychiatric symptoms, including progressive cognitive decline, regression, behavioral, and personality changes, social withdrawal, psychosis, confusion, and dementia (Nguyen et al., 2022).

### *Clinical Diagnostics of cblC*

Multiple organs are affected in *cblC* syndrome due to the multisystemic damage. Diagnosis is challenging due to its diverse symptoms that can present nonspecifically. The hallmark features of the disease are high levels of methylmalonic acid (MMA) in urine and blood, in addition to an increased total of homocysteine (tHcy) in plasma. Genetic identification of biallelic pathogenic variants in the *MMACHC* gene confirms the diagnosis. Treatment with injectable hydroxycobalamin supplement improves survival and can reduce, but not eliminate, primary biochemical manifestations (Sloan et al., 2020). If pathogenic variants in the family are known, treatment is started in utero or as soon as possible after birth, but most mutations are *de novo*.

Nevertheless, the craniofacial and cognitive phenotypes manifest during the early stages of development and generally cannot be improved through treatment (Ahrens-Nicklas et al., 2017; Scalais et al., 2023; Trefz et al., 2016).

***Mutations identified in the MMACHC gene***

There are more than 50 known mutations identified in the *MMACHC* gene that cause *cblC* disease, pathogenic variants are summarized in Table 1, 2, 3. The most frequent is c.271dupA (p.R91KfsX14), a frameshift mutation that accounts for at least 40% of disease-causing alleles which causes a frameshift mutation at codon 91 and a premature termination at codon 105 (Carrillo-Carrasco et al., 2012). The second most common mutation, c.394C>T (p.R132X), represents 20% of affected alleles. Individuals with c.394C>T tend to present with late onset disease, whereas patients with c.271dupA tend to present in infancy. Moreover, in the published cases of patients homozygous for c.271dupA mutation the phenotype was invariably early onset (Frattini et al., 2010). Many patients with early-onset, severe disease have the c.271dupA or the c.331 C>T (p.R111X) mutations in the homozygous or compound heterozygote state (Table 3). Mutations usually associated with a late-onset presentation include c.394 C>T (p.R132X) and c.482 G>A (p.R161Q) (Table 1). This mutation results in highly morbid, early onset disease when present in homozygous form. When c.271dupA is present in a compound heterozygous state, the phenotype depends on the characteristics of the second mutation. For example, individuals with c.271dupA and c.394C > T tend to present with disease after the first year of life (Lerner-Ellis et al. 2009). However, even in siblings who share pathogenic variants in *MMACHC* with similarly elevated Hcy and MMA, clinical presentations can differ, suggesting additional genetic or environmental factors at play (Higashimoto et al. 2019).

Table 1. Frameshift mutations that cause *cblC*

| Name | Gene(s) | Protein change | Condition(s) | Clinical significance (Last reviewed) |
|---|---|---|---|---|
| NM_015506.3(MMACHC):c.123dup (p.Pro42fs) | MMACHC | P42fs | Cobalamin C disease | Pathogenic(Last reviewed: Aug 31, 2021) |
| NM_015506.3(MMACHC):c.14_24del (p.Val5fs) | MMACHC | V5fs | Cobalamin C disease | Pathogenic(Last reviewed: May 28, 2022) |
| NM_015506.3(MMACHC):c.151_152del (p.Leu51fs) | MMACHC | L51fs | Cobalamin C disease | Pathogenic(Last reviewed: Feb 8, 2022) |
| NM_015506.3(MMACHC):c.187del (p.Leu63fs) | MMACHC | L63fs, L6fs | Cobalamin C disease | Pathogenic(Last reviewed: Dec 23, 2021) |
| NM_015506.3(MMACHC):c.285dup (p.Glu96fs) | MMACHC | E39fs, E96fs | Cobalamin C disease | Pathogenic/Likely pathogenic(Last reviewed: Aug 20, 2022) |
| NM_015506.3(MMACHC):c.310_313del (p.Asp104fs) | MMACHC | D47fs, D104fs | Cobalamin C disease | Pathogenic/Likely pathogenic(Last reviewed: Dec 9, 2022) |
| NM_015506.3(MMACHC):c.321_329delinsACACC (p.Asn110fs) | MMACHC | N110fs, N53fs | Cobalamin C disease | Pathogenic(Last reviewed: Apr 7, 2023) |
| NM_015506.3(MMACHC):c.328_331del (p.Asn110fs) | MMACHC | N53fs, N110fs | Cobalamin C disease | Pathogenic(Last reviewed: Oct 21, 2022) |
| NM_015506.3(MMACHC):c.352del (p.Gln118fs) | MMACHC | Q118fs, Q61fs | Cobalamin C disease | Pathogenic(Last reviewed: Jun 9, 2023) |
| NM_015506.3(MMACHC):c.364dup (p.His122fs) | MMACHC | H122fs, H65fs | Cobalamin C disease | Pathogenic(Last reviewed: Nov 27, 2018) |
| NM_015506.3(MMACHC):c.384del (p.Tyr129fs) | MMACHC | Y129fs, Y72fs | Cobalamin C disease | Pathogenic/Likely pathogenic(Last reviewed: Sep 1, 2021) |
| NM_015506.3(MMACHC):c.398_399del (p.Gln133fs) | MMACHC | Q133fs, Q76fs | Cobalamin C disease | Pathogenic/Likely pathogenic(Last reviewed: Oct 20, 2022) |
| NM_015506.3(MMACHC):c.433del (p.Ile145fs) | MMACHC | I145fs, I88fs | Cobalamin C disease | Pathogenic(Last reviewed: Jan 1, 2022) |
| NM_015506.3(MMACHC):c.434dup (p.Ser146fs) | MMACHC | S146fs, S89fs | Cobalamin C disease | Pathogenic/Likely pathogenic(Last reviewed: Nov 3, 2022) |
| NM_015506.3(MMACHC):c.435_436del (p.Ser146fs) | MMACHC | S146fs, S89fs | Cobalamin C disease | Pathogenic(Last reviewed: Oct 14, 2021) |
| NM_015506.3(MMACHC):c.445_446del (p.Cys149fs) | MMACHC | C92fs, C149fs | Cobalamin C disease | Pathogenic(Last reviewed: Oct 13, 2022) |
| NM_015506.3(MMACHC):c.48_49del (p.Cys17fs) | MMACHC | C17fs | Cobalamin C disease | Pathogenic(Last reviewed: Apr 26, 2020) |
| NM_015506.3(MMACHC):c.497dup (p.Pro167fs) | MMACHC | P167fs, P110fs | Cobalamin C disease | Pathogenic/Likely pathogenic(Last reviewed: Mar 14, 2022) |
| NM_015506.3(MMACHC):c.500del (p.Pro167fs) | MMACHC | P167fs, P110fs | Cobalamin C disease | Pathogenic(Last reviewed: Jul 10, 2022) |
| NM_015506.3(MMACHC):c.506_507del (p.Ile169fs) | MMACHC | I112fs, I169fs | Cobalamin C disease | Pathogenic(Last reviewed: Sep 1, 2021) |
| NM_015506.3(MMACHC):c.507_519del (p.Glu170fs) | MMACHC | E113fs, E170fs | Cobalamin C disease | Pathogenic/Likely pathogenic(Last reviewed: Jul 14, 2021) |
| NM_015506.3(MMACHC):c.534del (p.Lys178fs) | MMACHC | K178fs, K121fs | Cobalamin C disease | Pathogenic(Last reviewed: Aug 12, 2021) |
| NM_015506.3(MMACHC):c.547_548del (p.Val183fs) | MMACHC | V126fs, V183fs | Cobalamin C disease | Pathogenic(Last reviewed: Aug 9, 2022) |
| NM_015506.3(MMACHC):c.551_554dup (p.Arg186fs) | MMACHC | R129fs, R186fs | Cobalamin C disease | Pathogenic(Last reviewed: Oct 3, 2022) |
| NM_015506.3(MMACHC):c.565del (p.Arg189fs) | MMACHC | R132fs, R189fs | Cobalamin C disease | Pathogenic/Likely pathogenic(Last reviewed: Aug 12, 2022) |
| NM_015506.3(MMACHC):c.567dup (p.Ile190fs) | MMACHC | I190fs, I133fs | Cobalamin C disease | Pathogenic(Last reviewed: Jan 8, 2023) |
| NM_015506.3(MMACHC):c.603_604del (p.Asp202fs) | LOC129930446\|MMACHC | D145fs, D202fs | Cobalamin C disease | Pathogenic(Last reviewed: Dec 30, 2021) |
| NM_015506.3(MMACHC):c.619del (p.Asp207fs) | LOC129930446\|MMACHC | D150fs, D207fs | Cobalamin C disease | Pathogenic(Last reviewed: Jul 12, 2021) |
| NM_015506.3(MMACHC):c.619dup (p.Asp207fs) | LOC129930446\|MMACHC | D150fs, D207fs | not provided\|Cobalamin C disease | Pathogenic/Likely pathogenic(Last reviewed: Aug 16, 2022) |
| NM_015506.3(MMACHC):c.626_627del (p.Val209fs) | LOC129930446\|MMACHC | V209fs, V152fs | Cobalamin C disease | Pathogenic/Likely pathogenic(Last reviewed: Oct 14, 2021) |
| NM_015506.3(MMACHC):c.626dup (p.Thr210fs) | LOC129930446\|MMACHC | T153fs, T210fs | Cobalamin C disease | Pathogenic(Last reviewed: Oct 3, 2022) |
| NM_015506.3(MMACHC):c.648dup (p.Glu217fs) | LOC129930446\|MMACHC | E160fs, E217fs | Cobalamin C disease | Pathogenic(Last reviewed: Jun 8, 2022) |
| NM_015506.3(MMACHC):c.649_650del (p.Glu217fs) | LOC129930446\|MMACHC | E160fs, E217fs | Cobalamin C disease | Pathogenic(Last reviewed: Aug 31, 2021) |
| NM_015506.3(MMACHC):c.661_664dup (p.Tyr222fs) | LOC129930446\|MMACHC | Y165fs, Y222fs | Cobalamin C disease | Pathogenic(Last reviewed: Oct 7, 2022) |

Table 2. Nonsense Mutations that cause *cblC*

| Variation/location | Gene(s) | Protein change | Condition(s) | Clinical significance (Last reviewed) |
|---|---|---|---|---|
| NM_015506.3(MMACHC):c.217C>T (p.Arg73Ter) | MMACHC | R73*, R16* | Cobalamin C disease | Pathogenic(Last reviewed: Aug 20, 2022) |
| NM_015506.3(MMACHC):c.270dup (p.Arg91Ter) | MMACHC | R34*, R91* | Cobalamin C disease | Pathogenic(Last reviewed: Jun 8, 2016) |
| NM_015506.3(MMACHC):c.292C>T (p.Gln98Ter) | MMACHC | Q98*, Q41* | Cobalamin C disease | Pathogenic(Last reviewed: Aug 29, 2022) |
| NM_015506.3(MMACHC):c.315C>A (p.Tyr105Ter) | MMACHC | Y105*, Y48* | Cobalamin C disease | Pathogenic(Last reviewed: Sep 1, 2021) |
| NM_015506.3(MMACHC):c.315C>G (p.Tyr105Ter) | MMACHC | Y105*, Y48* | Cobalamin C disease | Pathogenic(Last reviewed: Sep 13, 2017) |
| NM_015506.3(MMACHC):c.331C>T (p.Arg111Ter) | MMACHC | R111*, R54* | Cobalamin C disease | Pathogenic(Last reviewed: Oct 7, 2022) |
| NM_015506.3(MMACHC):c.352C>T (p.Gln118Ter) | MMACHC | Q118*, Q61* | Cobalamin C disease | Pathogenic(Last reviewed: Apr 29, 2021) |
| NM_015506.3(MMACHC):c.394C>T (p.Arg132Ter) | MMACHC | R132*, R75* | cblC type of combined methylmalonic aciduria and homocystinuria\|not provided\|Cobalamin C disease\|Abnormality of metabolism/homeostasis | Pathogenic(Last reviewed: Feb 17, 2023) |
| NM_015506.3(MMACHC):c.419G>A (p.Trp140Ter) | MMACHC | W83*, W140* | Cobalamin C disease | Pathogenic(Last reviewed: Aug 31, 2021) |
| NM_015506.3(MMACHC):c.420G>A (p.Trp140Ter) | MMACHC | W140*, W83* | Cobalamin C disease | Pathogenic(Last reviewed: Oct 25, 2022) |
| NM_015506.3(MMACHC):c.457C>T (p.Arg153Ter) | MMACHC | R153*, R96* | Cobalamin C disease | Pathogenic(Last reviewed: Jul 1, 2023) |
| NM_015506.3(MMACHC):c.471G>A (p.Trp157Ter) | MMACHC | W157*, W100* | Cobalamin C disease | Pathogenic/Likely pathogenic(Last reviewed: Sep 14, 2021) |
| NM_015506.3(MMACHC):c.477_478insCATCCGAGGGGTAGTGCTGCTGCCAGGGATAGAGGTGCCAGATCTGCCACCCAGAAAACCTCATGACTGTGTACCTACAAGAGCTGAC (p.Ile160delinsHisProArgGlySerAlaAlaAlaArgAspArgGlyAlaArgSerAlaThrGlnLysThrSerTer) | MMACHC | | Cobalamin C disease | Pathogenic(Last reviewed: Aug 29, 2022) |
| NM_015506.3(MMACHC):c.481C>T (p.Arg161Ter) | MMACHC | R161*, R104* | Cobalamin C disease | Pathogenic(Last reviewed: Jan 11, 2023) |
| NM_015506.3(MMACHC):c.599G>A (p.Trp200Ter) | LOC129930446\|MMACHC | W143*, W200* | Cobalamin C disease | Pathogenic(Last reviewed: Apr 29, 2022) |
| NM_015506.3(MMACHC):c.600G>A (p.Trp200Ter) | LOC129930446\|MMACHC | W200*, W143* | Cobalamin C disease | Pathogenic(Last reviewed: Jul 6, 2022) |
| NM_015506.3(MMACHC):c.608G>A (p.Trp203Ter) | LOC129930446\|MMACHC | W203*, W146* | \|Cobalamin C disease | Pathogenic(Last reviewed: Apr 25, 2022) |
| NM_015506.3(MMACHC):c.609G>A (p.Trp203Ter) | LOC129930446\|MMACHC | W203*, W146* | \|Cobalamin C disease | Pathogenic(Last reviewed: Nov 3, 2022) |
| NM_015506.3(MMACHC):c.615C>A (p.Tyr205Ter) | LOC129930446\|MMACHC | Y205*, Y148* | Cobalamin C disease | Pathogenic(Last reviewed: Oct 3, 2022) |
| NM_015506.3(MMACHC):c.615C>G (p.Tyr205Ter) | LOC129930446\|MMACHC | Y205*, Y148* | Cobalamin C disease | Pathogenic(Last reviewed: Nov 2, 2022) |
| NM_015506.3(MMACHC):c.647_649del (p.Ser216_Glu217delinsTer) | LOC129930446\|MMACHC | | Cobalamin C disease | Pathogenic(Last reviewed: Oct 3, 2021) |
| NM_015506.3(MMACHC):c.666C>A (p.Tyr222Ter) | LOC129930446\|MMACHC | Y222*, Y165* | Cobalamin C disease | Pathogenic(Last reviewed: Dec 21, 2022) |
| NM_015506.3(MMACHC):c.89G>A (p.Trp30Ter) | MMACHC | W30* | Cobalamin C disease | Pathogenic |
| NM_015506.3(MMACHC):c.90_97del (p.Trp30_Glu33delinsTer) | MMACHC | | Cobalamin C disease | Pathogenic(Last reviewed: Sep 1, 2021) |
| NM_015506.3(MMACHC):c.90G>A (p.Trp30Ter) | MMACHC | W30* | Cobalamin C disease | Pathogenic/Likely pathogenic(Last reviewed: Aug 17, 2023) |

Table 3. Missense mutations that cause *cblC*

| Variation/location | Gene(s) | Protein change | Condition(s) | Clinical significance (Last reviewed) |
|---|---|---|---|---|
| NM_015506.2(MMACHC):c.482G>A | MMACHC | R161Q, R104Q | Inborn genetic diseases\|Cobalamin C disease | Pathogenic(Last reviewed: Apr 11, 2023) |
| NM_015506.3(MMACHC):c.182G>C (p.Arg61Pro) | MMACHC | R4P, R61P | Cobalamin C disease | Pathogenic/Likely pathogenic(Last reviewed: Aug 23, 2022) |
| NM_015506.3(MMACHC):c.1A>G (p.Met1Val) | MMACHC | M1V | Cobalamin C disease\|not provided | Pathogenic(Last reviewed: Sep 15, 2022) |
| NM_015506.3(MMACHC):c.276G>T (p.Glu92Asp) | MMACHC | E92D, E35D | Cobalamin C disease | Pathogenic(Last reviewed: Aug 28, 2021) |
| NM_015506.3(MMACHC):c.2T>G (p.Met1Arg) | MMACHC | M1R | Cobalamin C disease | Pathogenic/Likely pathogenic(Last reviewed: Jul 31, 2021) |
| NM_015506.3(MMACHC):c.347T>C (p.Leu116Pro) | MMACHC | L116P, L59P | Cobalamin C disease | Pathogenic/Likely pathogenic(Last reviewed: Sep 9, 2022) |
| NM_015506.3(MMACHC):c.388T>C (p.Tyr130His) | MMACHC | Y73H, Y130H | Cobalamin C disease | Pathogenic/Likely pathogenic(Last reviewed: Oct 24, 2022) |
| NM_015506.3(MMACHC):c.3G>A (p.Met1Ile) | MMACHC | M1I | Cobalamin C disease | Pathogenic(Last reviewed: Nov 3, 2022) |
| NM_015506.3(MMACHC):c.440G>A (p.Gly147Asp) | MMACHC | G147D, G90D | Cobalamin C disease | Pathogenic/Likely pathogenic(Last reviewed: Sep 23, 2022) |
| NM_015506.3(MMACHC):c.440G>C (p.Gly147Ala) | MMACHC | G147A, G90A | Inborn genetic diseases\|Disorders of Intracellular Cobalamin Metabolism\|Cobalamin C disease | Pathogenic/Likely pathogenic(Last reviewed: Aug 12, 2023) |
| NM_015506.3(MMACHC):c.449T>A (p.Ile150Lys) | MMACHC | I150K, I93K | Cobalamin C disease | Pathogenic(Last reviewed: Feb 2, 2022) |
| NM_015506.3(MMACHC):c.464G>A (p.Gly155Glu) | MMACHC | G155E, G98E | Cobalamin C disease | Pathogenic(Last reviewed: Aug 1, 2013) |
| NM_015506.3(MMACHC):c.471G>C (p.Trp157Cys) | MMACHC | W100C, W157C | not provided\|Cobalamin C disease | Pathogenic/Likely pathogenic(Last reviewed: Jun 21, 2021) |
| NM_015506.3(MMACHC):c.481C>G (p.Arg161Gly) | MMACHC | R161G, R104G | Cobalamin C disease | Pathogenic/Likely pathogenic(Last reviewed: Apr 19, 2022) |
| NM_015506.3(MMACHC):c.484G>T (p.Gly162Trp) | MMACHC | G105W, G162W | Cobalamin C disease | Pathogenic(Last reviewed: Nov 7, 2023) |
| NM_015506.3(MMACHC):c.565C>A (p.Arg189Ser) | MMACHC | R189S, R132S | Cobalamin C disease | Pathogenic/Likely pathogenic(Last reviewed: Nov 11, 2022) |
| NM_015506.3(MMACHC):c.578T>C (p.Leu193Pro) | MMACHC | L193P, L136P | Cobalamin C disease | Pathogenic(Last reviewed: Oct 3, 2022) |
| NM_015506.3(MMACHC):c.643T>C (p.Tyr215His) | MMACHC\|LOC129930446 | Y158H, Y215H | Cobalamin C disease | Pathogenic(Last reviewed: May 25, 2022) |
| NM_015506.3(MMACHC):c.80A>G (p.Gln27Arg) | MMACHC | Q27R | Cobalamin C disease | Pathogenic(Last reviewed: Jul 26, 2023) |

## COBALAMIN UPTAKE, PROCESSING, AND UTILIZATION IN CELLS

Cobalamin or vitamin B12 (Cbl; B12) is an important cofactor in homocysteine metabolism and in branched amino acid and odd-chain fatty acid catabolism (Lerner-Ellis, et al., 2006). It is a water-soluble micronutrient that is synthesized exclusively by a group of microorganisms. Vitamin B12 from the diet comes in three chemical forms. Such as hydroxocobalamin, methylcobalamin, and adenosylcobalamin. B12 that is found is supplements is known as cyanocobalamin (Hannibal & Jacobsen, 2022).

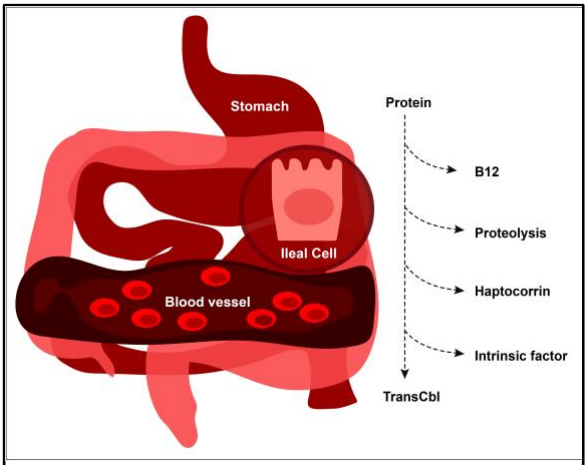


Figure 1.1. Vitamin B12 absorption. After the ingestion of B12, the vitamin undergoes proteolysis, where it then binds to haptocorrin released from the salivary glands. After the separation of this complex, B12 then is bound to intrinsic factor and taken up by the ileal. A complex is created known as TransCbl, where it routes itself to be absorbed into cells and further metabolized.

After ingestion B12 is released from its protein carrier by proteolysis. During this time there is a secretion of haptocorrin from the salivary glands to where it then anchors onto Cbl to prevent any damage caused by acidic conditions of the stomach. After the release from haptocorrin, Cbl is then bound to intrinsic factor to be transported to the ileum where apical membrane intestinal epithelial cells of the brush-border incorporate it via receptor mediated endocytosis (Figure 1.1). The intrinsic factor-Cbl complex is internalized after binding to the receptor known as cubam, then dissociation of the complex occurs to degrade intrinsic factor (Kósa et al. 2022).

After absorption B12 is distributed to every cell in the body by a second carrier protein known as transcobalamin (TCbl). The joining of the two enables it to be accessible for cellular

absorption through endocytosis mediated by the cell surface transcobalamin receptor (TCblR). TCbl uptake is degraded in the lysosome, and the resulting Cbl is then released into the cytoplasm through the lysosomal membrane to undergo enzyme-mediated reduction (Figure 1.2). Cbl released into the cytoplasm binds to *MMACHC*. The gene is responsible for accelerating the removal of the upper axial ligand of Cbl. MMACHC encodes a protein that serves as a cobalamin processing enzyme. It is required for both the trafficking of Cbl within the cytoplasm and the decyanation and dealkylation of Cbl derivatives (Figure 1.2).

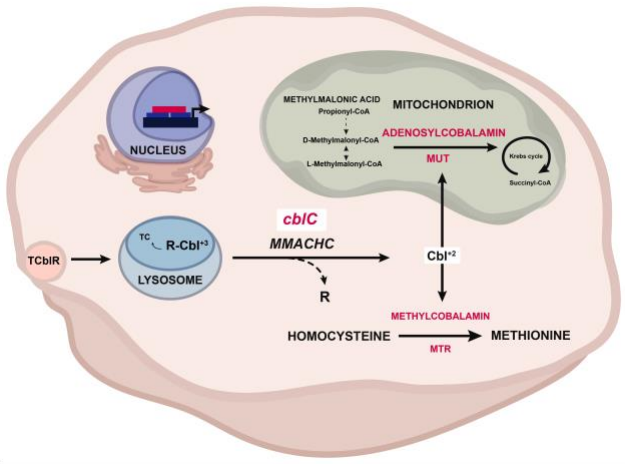


Figure 1.2 Cobalamin cell metabolism
Cbl is taken up by the TCbR where TCbl is transported into the lysosome to be degraded. Cbl is released into the cytoplasm where branches into two separate pathways; that of the mitochondrion or cytoplasm to be converted into its active form.

**Methylmalonic Acidemia and homocystinuria (MMACHC)**

*cblC* is caused by mutations in the *MMACHC* gene. The *MMACHC* gene is located at 1p34.1 and consists of five exons. It encodes a protein of 282 amino acids with a predicted molecular weight of 31.7 kDa (Lerner-Ellis et al., 2006). *MMACHC* includes 10,736 bp of genomic DNA. According to Lerner-Ellis et al. (2006), the gene has a high degree of conservation across mammalian species and does not appear to have any comparable proteins in prokaryotes. MMACHC is an enzyme that exhibits versatility in its function, as it is capable of converting cobalt-carbon bonds (specifically, 5'-deoxyadenosyl-, cyano-, or hydroxyl groups such as OHCbl) through either homolytic or heterolytic cleavage. Although this disorder has been demonstrated to

be a heterogeneous condition, identification of the gene involved has allowed study of phenotype-genotype correlation. Mutations in *MMACHC* result in reduced production of AdoCbl and MeCbl and a decrease in methylmalonyl- CoA mutase (MUT) and methionine synthase (MTR) activity. This decrease in B12 derived cofactors leads to an increase in the upstream metabolites MMA and homocysteine (Hcy), due to reduced overall enzyme function of MUT and MTR (Lerner-Ellis et al., 2006). Concurrently, methionine synthesis is reduced overall.

***Methylcobalamin***

MeCbl plays a crucial role in the cytosolic environment by facilitating the remethylation process of homocysteine into methionine which is facilitated by MTR (Figure 1.2). Methionine is the direct metabolic precursor to S-adenosylmethionine, which is the ubiquitous methyl donor in the transmethylation process of DNA, histones, and other proteins and small molecules (Chern et al., 2020). Furthermore, methionine production plays a critical role in the synthesis of nucleic acids, neurotransmitters, and phospholipids. Therefore, the decrease in methionine production observed in *cblC* disrupts various cellular processes (Chern et al., 2020).

***Adenosylcobalamin***

Cbl is an essential micronutrient that is intrinsically linked to the interdependent metabolic pathways of the folate cycle, methionine cycle, and S-adenosyl methionine. In the mitochondrion, AdoCbl functions as a cofactor for MUT (Figure 1.2) (Chern et al., 2020). This facilitates the conversion of L-methylmalonyl-CoA to succinyl-CoA, which is the ultimate step in the anaplerotic replenishment of the tricarboxylic acid cycle through the catabolism of branched-chain amino acids, odd-chain fatty acids, and the side chain of cholesterol. (SAM)-dependent methylation and catabolism of odd-chain fatty acids and branched-chain amino acids. Elevated levels of MMA in plasma may be associated with developmental delay because of an increase in odd-chain fatty acid

assimilation and trapping of toxic metabolites within neurons. However, this hypothesis has not been directly tested.

## NEURODEVELOPMENTAL IMPAIRMENT IN *CBLC*

Early-onset *cblC* syndrome accounts for 90% of all reported cases (Nguyen et al., 2022). Global developmental delay (GDD) and intellectual disability (ID) are the most prevalent features of early onset *cblC* (Nguyen et al., 2022). The neurodevelopmental phenotypes associated with *cblC* can be severe. This is largely due to the critical role Cbl plays in the synthesis of fatty acids, amino acids, neurotransmitters, and DNA/RNA. There is a strong genotype-phenotype correlation with regards to age of onset. Phenotypic differences may be due to the mutational spectrum of *MMACHC*.

### Inability to treat early onset presentations.

Neurological phenotypes manifest early in development and therapeutic interventions such as hydroxycobalamin supplementation cannot ameliorate symptoms. For example, in a case study of an infant with early onset *cblC*, the clinical presentations were worsening symptoms of sensory peripheral demyelinating neuropathy (Frattini et al., 2010). Electrophysiological tests revealed a uniform and symmetric slowing of sensory and motor conduction velocities in the lower limbs and the absence of sensory nerve action potentials. In addition to this, there were also reports of feeding difficulties, severe hypotonia, converging strabismus, and psychomotor delay (Frattini et al., 2010). Treatment with oral hydroxycobalamin, vitamin B6, folic acid, carnitine, and betaine had reduced metabolite levels but failed to normalize or demonstrate clinical improvement (Frattini et al., 2010).

However, other cases studies have shown some efficacy for successful intervention depending on the onset of treatment. A case study published by Trefz et al. (2016) presented data

for two siblings with *cblC* syndrome treated with a cobalamin derivative, hydroxycobalamin, at different ages. Among the results, the siblings had different manifestations of clinical symptoms. For example, sibling 1 received treatment four months after birth, while sibling 2 was treated intrauterine at 15 weeks of pregnancy. The clinical outcomes were drastically different. Sibling 1 had severe clinical presentations of intellectual disabilities and ophthalmic symptoms. Sibling 2 had mild ophthalmic issues and an average IQ was reported at an 11-year follow-up. The study suggests that early intrauterine treatment can positively impact the outcome of *cblC* defects (Trefz et al., 2016). Although there were positive outcomes, sibling 2 still had slight abnormalities in the development of white matter suggesting that some brain phenotypes may occur independent of cbl availability. These data also may suggest that MMACHC is a versatile protein, with multiple functions. This further suggests that the resulting brain phenotypes are manifesting during early developmental timepoints.

***Brain Malformations***

Unsurprisingly, little is known about the many types of developmental disability and its neurobehavioral manifestations. On top of that, they are not well characterized. The only case study that has tried to somewhat interlink the two was reported by Chen et al. (2022), where they investigated the intellectual age in relation to development. They looked at five aspects: gross motor movements, fine movements, adaptability, language, and social behavior (Chen et al., 2022). This study identified brain malformations by magnetic resonance imaging that were correlated with delayed development in patients. The most common abnormalities observed were ventricular dilation, cerebral atrophy, and corpus callosal thinning (Chen et al., 2022). Although these features are common and often the most severe deficits, there were no specific criteria for predicting the

prognosis of *cblC* defect and no single brain region was directly correlated with other clinical phenotypes.

***Intellectual disabilities***

Intellectual impairment is also commonly observed along with gross morphological changes in the brain. The case studies by Beauchamp et al. (2009) involved the longitudinal assessment of two patients diagnosed with *cblC* disease using standardized neuropsychological tests. According to Beauchamp et al. (2009), the patients demonstrated cognitive impairment, attention deficits, and a progressive decline in intellectual functioning. Patient 1 was 12 years old and diagnosed with *cblC* at the age of 3 weeks and underwent a treatment regimen that includes protein restriction, injections of hydroxycobalamin, betaine supplementation, and folic acid administration. Despite vitamin supplementation intellectual ability progressively deteriorated, as well as vision impairment caused by cone-rod dystrophy and delayed development. These data suggest not all brain phenotypes can be solely the result of abnormal cbl metabolism or the accumulation of toxic metabolites. The individual exhibits deficits in attention, executive function, and adaptive skills. Patient 2 age 12, who received a diagnosis of *cblC* disease at four weeks of age. The individual in question received comparable levels of care and has demonstrated steady, albeit modest, advancements in their development. In addition, patient 2 showed deficits in attention, executive function, and adaptive abilities, while displaying relative proficiencies in social skills. Both patients have a consistent trend of diminishing cognitive abilities over a period of time, which may be related to deficits in attention and executive function despite having been supplement with various forms of cbl and other metabolites (betaine, folic acid) (Beauchamp et al., 2009).

***Atypical Behavior***

Most cognitive or behavioral deterioration in *cblC* occurs in the late-onset form of the disease. Their clinical presentations are less severe and have a much better prognosis. Since neurodevelopmental deficits are quite severe in the early-onset form of *cblC* syndrome, it is challenging to investigate the extent of these manifestations while considering gross morphological changes in brain development. Only one case study has evaluated other developmental domains that have linked psychiatric decline with *cblC* syndrome in the development of anxiety or depression. An adolescent patient presented comorbidities of autism spectrum disorder (ASD) and attention deficit and hyperactivity disorder (ADHD) with decompensation in behavior. The patient was reported to have developmental delays with poor fine motor skills and receptive/expressive language disorder, ASD, ADHD, strabismus, nystagmus, and myopia. He started treatment at 1 month of age with hydroxocobalamin, folic acid, carnitine, and mild protein restriction and began treatment with betaine at 6 months. The patient's family documented that the patient followed the prescribed medication regimen. However, the patient experienced a decline in cognition and was hospitalized for treatment following an episode. In addition to pacing and being uncooperative, the patient exhibited "aggressive behavior" and "psychosis/hallucinations." This was the first case study to establish a relation between *cblC* syndrome and psychiatric decline, including the development of anxiety and depression.

***MMA and Hcl are associated with cognitive decline***

The pathophysiology that underlies the neuropsychiatric disturbances observed in *cblC* disease is still poorly understood. High levels of MMA and Hcl, in conjunction with low levels of MET, have been associated with an increased risk of developing microangiopathic diseases. Elevated levels of Hcl are also associated with declining cognitive performance in elderly adults

due to damage of vascular endothelium and excessive N-methyl-D-aspartate, NMDA, stimulation (Weisfeld-Adams et al., 2013). Elevated levels of MMA in plasma may be associated with developmental delay due to increased assimilation of odd chain fatty acids and the trapping of toxic metabolites within neurons. However, the high levels of MMA and Hcl seen in vitamin B12 deficiency do not account for many symptoms seen in *cblC* (Weisfeld-Adams et al. 2013).

### *Dysmorphic features in cblC*

A subset of patients with *cblC* have been reported to have mild to moderate atypical facial development. In a case report published by Cerone et al. (1999), the development of 13 early-onset *cblC* patients were monitored and reports show that 7 of the 13 patients had minor facial anomalies. These were characterized by a long face, high forehead, a flat philtrum, and a low set of large ears. The earliest age observed to present distinguishable facial features was a female patient at 2 months of age who had shown a high forehead and low set ears, at the age of 2 months (Cerone et al., 1999). The morphological characteristics were more apparent after 3 years of age. The morphological anomalies were similar in each patient (Cerone et al., 1999).

## FINDING A MODEL TO CHARACTERIZE EARLY DEVELOPMENTAL PHENOTYPES

In 2014 Quintana et al. demonstrated that knockdown of *mmachc* in zebrafish caused abnormal facial development. The phenotypes were more severe than those found in patients but suggested that *mmachc* regulates craniofacial development, however, metabolites were not abnormal, suggesting that at least some of the facial phenotypes were not a direct consequence of B12 binding and enzyme activity (Quintana et al., 2014). There have been attempts to generate Cbl-deficient mice; however, embryos were unable to grow through embryonic day 3.5 (Chern et al., 2020). One model was a conditional knockout mouse *Mmachc* floxed allele ($Mmachc^{flox/flox}$) that allowed tissue-specific deletion of the *Mmachc* gene. The second model is a transgenic mouse

line that overexpresses functional *Mmachc* (Mmachc$^{-OE+/8}$). Severe craniofacial dysmorphia, microphthalmia or anophthalmia, exencephaly, wavy spinal cord, and thin hypertrabeculated ventricles with ventricular septum defects were observed in mice knockout animals. The impact of *MMACHC* loss of function on the development of the central nervous system, craniofacial skeleton, and eyes is reflected in these anomalies. *Mmachc* germline mutant mice had severe developmental defects and mutation was embryonic lethal.

**Zebrafish germline mutation of *mmachc***

To model the phenotypic and biochemical characteristics of patients with *cblC*, including growth impairment, developmental delay, manifestation of retinopathy and accumulation of organic acids, specifically elevated MMA. Sloan et al. (2020) identified the zebrafish orthologue of *MMACHC* and then used zinc finger nucleases (ZFN) to create a nonsense germline mutant of *mmachc.* The zebrafish orthologue of *MMACHC*, shares 51% sequence identity with the human protein but diverges at the C-terminus, resulting in a shorter protein of 250 versus 282 amino acids in human. Sloan and colleagues characterized the zebrafish *mmachc*$^{hg13/hg13}$ allele, which results in an insertion/deletion and premature stop codon (Figure 1.3). Consequently, the model demonstrated phenotypic and biochemical similarities as those seen in *cblC* patients, such as metabolite accumulation, developmental delays, growth restriction, and organic acid accretion (Sloan et al., 2020). ZFNs were used to target exon 2 for mutagenesis because this location is close

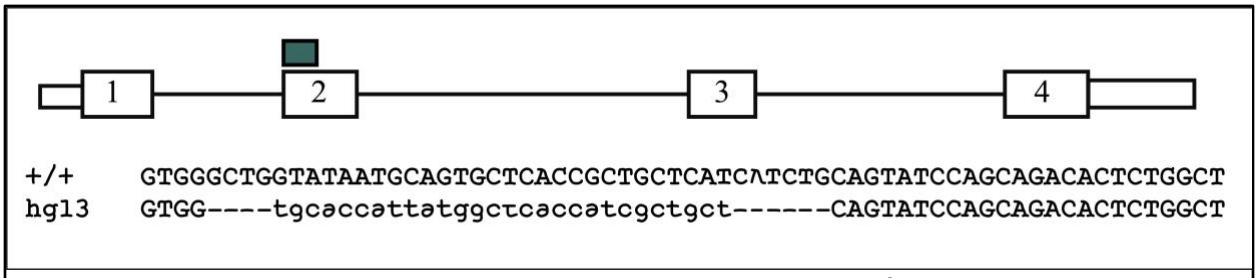


Figure 1. 3 hg13 allele is an insertion/deletion in the zebrafish *mmachc* gene. The mutation introduces a premature stop codon and was characterized by Sloan and colleagues in 2020.

to the homologous position of a severe and common human pathogenic variant, c.271dupA p.Arg91Lysfs∗14. The hg13 allele results in a net 10 base pair deletion; c.95_132delins28 p.Gly32Valfs∗48, in the gene causing a loss of function (Figure 1.3). The allele is a frameshift mutation predicted to cause nonsense-mediated decay of the corresponding mRNA. Quantitative PCR (qPCR) showed that *mmachc* RNA levels were undetectable in $mmachc^{hg13/hg13}$.

### DANIO RERIO: A POWERFUL MODEL FOR NEURODEVELOPMENT

The zebrafish (*Danio Rerio*), a freshwater teleost, is a low-cost and easy-to-maintain organismal model for genetic, behavior, and pharmacological studies (Adamson et al., 2018; Audira et al., 2018; Basnet et al., 2019; Curpăn et al., 2022; De Abreu et al., 2020; Kalueff et al., 2014). They are genetically and physiologically similar to humans, making them well suited for their capacity for large-scale phenotypic and therapeutic screening, and they are highly amenable to the generation disease models through genome editing technologies (Adamson et al., 2018; Curpăn et al., 2022; Howe et al., 2013; Stewart et al., 2014). More importantly, they have a quick developmental timeline. Furthermore, zebrafish are an established model system for studying rare diseases and behavioral studies involving neurodevelopmental disorders (NDD) (Adamson et al., 2018; Breuer & Patten, 2020).

Zebrafish have also served as a powerful tool for studying orofacial abnormalities, including that of the cleft lip/cleft palate (Li et al., 2022; Rai et al., 2022; Raterman et al., 2020). One example includes studies involving early development that have surmised that the overuse of acetaminophen or paracetamol can lead to the development of morphological abnormalities in craniofacial structures (Rai et al., 2022). Most importantly, mutation of *mmachc* in zebrafish is lethal weeks post fertilization after much of development has been completed. This contrasts with

mice, that are embryonic lethal precluding some behavioral studies. Survival can likely be attributed to maternal deposition of *mmachc* encoding mRNA.

## ZEBRAFISH LARVAE TO STUDY NEURODEVELOPMENTAL DISORDERS

Zebrafish are now being used more often to study complex behaviors. Most of the behavioral tests used have already been validated in rodent models. However, zebrafish have distinct advantages when performing large-scale behavior analysis—specifically, their high fecundity, transparent development, and the homology they share with genetic diseases. In addition to the technical aspects, zebrafish larvae also follow the principles of replacement, reduction, and refinement. Larval zebrafish are more amendable to rapid throughput testing than adults and the developing nervous system is more sensitive to chemical insults. The animal model system has been used to investigate neurodevelopmental disorders such as attention deficit/hyperactivity disorder (ADHD), autism spectrum disorders (ASD), and intellectual disabilities (ID), with paramount evidence for its translational lessons to selected NDDs chosen based on the Diagnostic and Statistical Manual of Mental Disorders (DSM-V) (Dougnon & Matsui, 2022; Vaz et al., 2019). For example, zebrafish mimic the pathological effects of ASD which can reveal alterations in brain development, cell proliferation, neurogenesis, behavioral and genomic changes in embryonic and larval zebrafish (Basnet et al., 2019). Common phenotypes associated with ADHD include inattention, impulsiveness, and hyperactivity which all can be evaluated in zebrafish. Relevant to modeling ID, ethanol exposure during neurodevelopment induces learning and memory deficits in zebrafish.

### Structural and functional homology of the brain

The structural organization and cell morphology of the zebrafish brain is similar to rats and humans (Basnet et al., 2019). Zebrafish provide a platform among vertebrate model systems to

study the connection between different brain areas with behavior. Many structures, such as retina, olfactory bulb, cerebellum, and spinal cord, are similar in architecture in zebrafish and other vertebrates. Besides structural homology, the zebrafish brain is similar to humans and rodents with respect to neurochemistry. The zebrafish brain contains all the major components required for neurotransmission, such as neurotransmitter receptors, transporters, and enzymes of synthesis and metabolism. It also has the same neurotransmitter system as that of higher vertebrates such as GABA, glutamate, dopamine, noradrenaline, serotonin, histamine, and acetylcholine. Among the various neurochemical pathways, several pathways involved in the modulation of behavior in zebrafish have been well characterized.

Another important point to mention is that human disease shows molecular and structural homology in zebrafish. The habenula and amygdala like structure in zebrafish, for example, play a function in the regulation of affective responses like those seen in humans and rodents. The habenula regulates serotonin and dopamine release and is evolutionarily conserved (Basnet et al. 2019). It has also been observed that habenula hyperactivation causes similar symptoms when

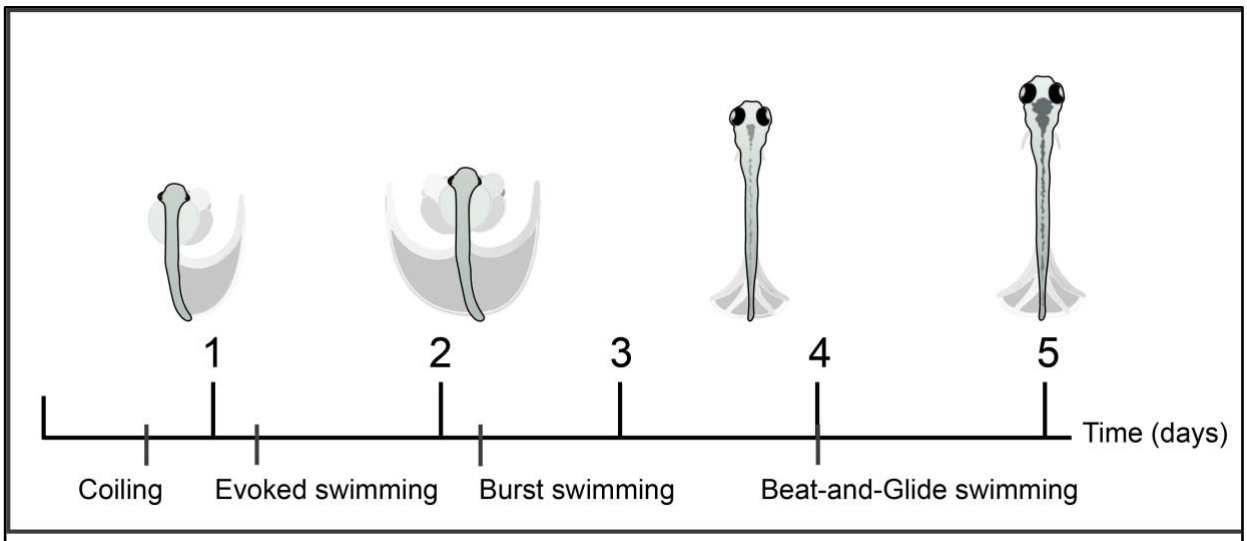


Figure 1.4. The larval swimming behavior undergoes further development within a few days. Within a few days, zebrafish larvae exhibit progressively complex movement patterns, which can offer valuable insights on abnormal neurodevelopment.

compared with depression and stress-related behaviors mammals. Zebrafish, unlike mammals, lack the neocortex, which is the primary region responsible for regulating executive processes, which are typically impaired in psychiatric disorders. However, research has demonstrated that zebrafish, a species of vertebrate with a smaller brain and no neocortex, are capable of complex decision making and cognitive processing (Basnet et. al. 2019).

### CHARACTERIZING ZEBRAFISH SWIM PATTERNS AS A READ OUT FOR NERVOUS SYSTEM DEVELOPMENT

The first behavior observed during zebrafish development is spontaneous movement beginning at 17 hours post fertilization (hpf), during which embryos perform slow alternating tail coils (Figure 1.4). The significance of this behavior stems from the fact that some neuro-deficits in zebrafish models are characterized by impaired stimuli response. The basic brain signaling systems of zebrafish, which are ontogenetically homologous to mammalian systems, form between 18 and 32 hpf. After 24 hpf, primary neurons arise and mediate early escape reflex activity, which is characterized as coordinated larval behavior provided by basic neural networks (De Abreu et al., 2020). Embryos within the chorion show rhythmic movement of the pectoral fins and can produce a startle response to a pulse of light. The larvae also demonstrate touch-induced responses that are facilitated by sensory neurons and are capable of coordinated swimming. The second stage of neurogenesis proceeds at the time of hatching (2-3 days post fertilization (dpf)), where muscular movements from reflex behavior occurs and as does the transition to more complex survival behaviors and movements (De Abreu et al., 2020).

When the constituents of each segment of the primary central nervous system differentiate and acquire functionality, the primary circuitry is replaced with second wave neurogenesis. However, escape response-type swimming behavior could be observed in prematurely

dechorionated embryos (2 dpf or even earlier), as brain-controlled movements in response to external stimuli can be seen as early as 2 dpf (De Abreu et al., 2020). As a result, brain impairments linked to abnormal locomotion patterns can be assessed as early as the larval stage.

**Motor development and behavior profiling in zebrafish larvae**

At 4-5 dpf, the swim bladder gradually inflates and at this developmental stage, larvae have excellent vision to hunt for food. After quick maturation of the sensory and motor system, zebrafish larvae can display more robust and complex behaviors within the first week of development. At 5 dpf zebrafish larvae display autonomous locomotion and demonstrate various behaviors such as hunting, escape, and avoidance (Orger & De Polavieja, 2017). They also exhibit photo-motor responses when subjected to rapid changes in light and dark conditions. Furthermore, after being exposed to strobe light stimuli, these zebrafish exhibit anxiety-like behavior. The motor behavior observed in zebrafish larvae can be distinguished by the occurrence of autonomous contractions in the tail region. During the subsequent hours, the activity patterns undergo a developmental process where in uncorrelated bursting patterns transition into coordinated side-to-side alternation. As larvae develop, they exhibit a range of motor behaviors including escape responses, swimming patterns, phototaxis, hunting and feeding activities, as well as optomotor responses.

**Automated systems for studying locomotor assays**

Zebrafish larval locomotor assays can be used as screening tools for testing the behavioral effects of many drugs, chemicals and toxins causing hyper- or hypoactivity from a safety pharmacology perspective. This can be assessed by monitoring behaviors of multiple animals at the same time using an automated imaging and motion tracking system. Therefore, the various automated systems that have been developed to study rodent behavior have been adapted to the study of zebrafish behavior (Champagne et al. 2010). Using these automated systems, various

behaviors can be studied in detail with the help of high-resolution video recordings and analytical software. A range of anxiolytic and stimulant compounds have been tested on locomotor activity of zebrafish larvae and were shown to produce responses like those seen in mammals. These zebrafish behaviors were later translated to larval/juvenile zebrafish (Tegelenbosch et al., 2012).

## CHARACTERIZATION OF BEHAVIOR REPERTOIRE

The characterization of behaviors observed in zebrafish larvae comparable to the adult zebrafish and rodents have increased the scope of their utility in the field of neuroscience. The larval stage of zebrafish begins at 72 hpf and development continues into the juvenile stage. During this period, zebrafish possess a vast amount of behaviors which could be analyzed automatically or manually and quantitatively or qualitatively (Basnet et al., 2019). Specifically in neuropharmacology, the behavior repertoire of zebrafish larvae has been utilized in a multipurpose way, such as identifying, repurposing, and discovery of drugs with central nervous system effect. This has included those for various psychiatric illnesses such as anxiety and mood disorders (Basnet et al., 2019).

### Modeling affective states

Zebrafish can be used for studying affective disorders by exploiting behavioral traits of survival. Anxiety disorders are frequently investigated in zebrafish because of their capacity to display behaviors resembling anxiety and the ease with which experimental protocols and assays can be implemented. These protocols and assays are comparable to those used with established rodents. In modeling the pathogenesis of affective states in fish, neurochemical and endocrine biomarkers of anxiety in zebrafish are frequently employed in conjunction with behavioral endpoints.

This includes ‘thigmotaxis’ and ‘boldness’ behavior (Kalueff et al., 2013). Interestingly, studies have shown that domesticated laboratory strains of zebrafish can diverge greatly from wild counterparts (Axling et al., 2022). For example, laboratory strains of zebrafish have shown pronounce differences in behavior, such as ‘boldness’ compared to their wild counterparts. This behavior is characterized as ‘risk-taking’ and presents itself in fish as having reduced anxiety.

***Bold or Risk taking behavior***

Behavior can be characterized as having a bold trait when discussing risk-taking behavior regarding zebrafish. It is also a known measurement for anxiolytic behavior. This can also be labeled as risk-taking behavior. Tests that measure an increase in exploratory activity, approaches to novel objects or engaging in dangerous situations can measure both bold and risk taking behavior (Kalueff et al., 2013). The open field test is a popular behavioral assay for determining boldness in fish and rodents. In this test, bold animals spend more time in the open region at the center of the arena.

***Thigmotaxis “wall hugging”***

Zebrafish larvae present thigmotaxis at 5 dpf. Thigmotaxis can be defined as showing a preference for staying near an edge or side, while avoiding open areas (Kalueff et al., 2013). For that reason, it is also referred to as wall-hugging behavior. It has been used as a valid index of anxiety and is evolutionarily conserved across different species, such as fish, rodents, and humans (Basnet et al., 2019; Kallai et al., 2007; Kalueff et al., 2013; Kalueff & Stewart, 2012). This is a phylogenetically old and energetically inexpensive exploratory strategy (Kallai et al., 2007; Kalueff & Stewart, 2012). When an animal initially explores an enclosed place, it tends to stay in close contact with the perimeter of that space. Avoiding the inner zone of an open field can be quantified by measuring the amount of time or path length that an organism spends in close contact

with the wall. Thigmotaxis as defined above is a primordial, genetically grounded type of behavior and an ecologically important strategy used by humans and other animals for spatial exploration mainly in open-field and arena maze experiments (Kallai et al., 2007). The use of anxiolytic drugs (i.e., diazepam) and anxiogenic drugs (i.e., caffeine) have been shown to attenuate and enhance thigmotaxis in larval zebrafish. Therefore, thigmotaxis can be a valid and critical measurement for studying anxiogenic and anxiolytic drugs (Basnet et al. 2019).

***Habituation***

Habituation is a non-associative form of learning in which a repeated stimulus leads to an attenuated response (Basnet et al. 2009). It is evolutionarily conserved and serves a role by which the nervous system filters irrelevant stimuli. Defective habituation is associated with several neuropsychiatric diseases such as schizophrenia and ADHD. Habituation studies could be used for the high-throughput screening of new compounds with specific effects on non-associative learning increased exploratory behavior (Kalueff et al., 2013).

***Locomotor Behavior***

Zebrafish larvae show mature swimming at 4–5 dpf following the development of a swim bladder. Locomotion in zebrafish is a complex behavior produced by the activity of various neurons, such as the reticulospinal neurons of the brain stem along with descending vestibulospinal or neuromodulatory projections (Basnet et al. 2019). All these pathways are evolutionarily conserved among vertebrates. The precision analysis of locomotion in zebrafish larvae with high-throughput methods could provide accurate information needed for the screening and identification of neuroactive compounds. There are various locomotor behavioral assays used for identifying neuroactive drugs. Among them is the light-dark locomotion test in which the locomotor activity and movement pattern of zebrafish larvae are analyzed via high-throughput automatic tracking.

Larvae are placed in multi-well plates inside a closed chamber and exposed to alternating light and dark conditions following a period of acclimatization. The distance travelled and the pattern of movement of zebrafish larvae in each of the conditions is evaluated for understanding the neurobehavioral effects. Zebrafish larvae show a specific pattern of movement when exposed to alternating light and dark conditions (Basnet et al. 2019). In this behavioral assay the light-dark transition increases locomotor activity whereas the dark-light transition decreases locomotor activity in zebrafish larvae. The increases observed in locomotor activity upon the light-dark transition are attributed to the increased stress/anxiety level in zebrafish larvae (Basnet et al., 2019). Collectively, these locomotor activities depend on the integrity of brain function, nervous system development, and visual pathways (Basnet et al., 2019).

**CRANIOFACIAL FORMATION IN ZEBRAFISH**

The craniofacial skeleton consists of the neurocranium and the viscerocranium (Figure 1.5). Both are composed primarily of cartilage elements that are later replaced by bone. Zebrafish larval cartilages are only a few cell layers thick and can be visualized by staining with alcian blue or using fluorescent transgenic reporters expressed in chondrocytes (Mork & Crump, 2015). Craniofacial development involves the formation and transformation of various structures in the head and face. Many of these structures are formed by neural crest cells (NCCs). These multipotent cells arise during brain development at the dorsal end of the neural tube, a structure that will become the vertebrate spinal cord. NCCs migrate away from the

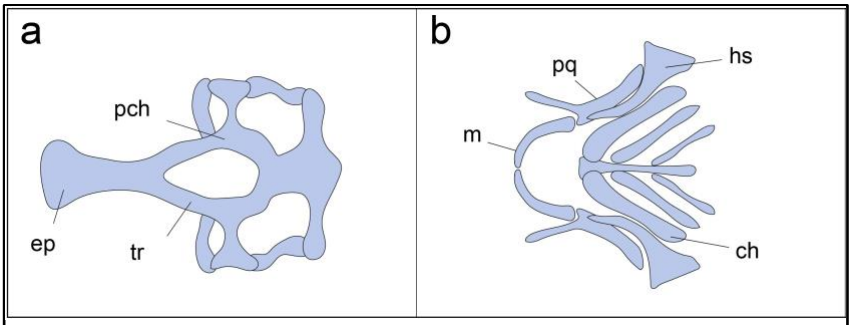


Figure 1. 5 Schematic of key craniofacial skeletal elements. The neurocranium (a) and viscerocranium (b) are skeletal elements that make up the mandible of the zebrafish.

dorsal end of the neural tube and produce multiple tissues including bones, cartilage, muscles, connective tissues, sensory ganglia, and pigment cells. The viscerocranium is derived from cranial NCCs that populate the seven pharyngeal arches (transient structures during development) of the zebrafish embryo, with multiple skeletal elements forming along the dorsal–ventral axis of each arch (Figure 1.5b). A subset of NCCs from the midbrain migrate anteriorly between and around the eyes to contribute to the neurocranium whereas posterior midbrain and hindbrain derived NCCs segregate into distinct streams that migrate ventrally into the pharyngeal arches (PA) to produce the viscerocranium. NCCs that migrate from the midbrain and rhombomeres 1-3 contribute to the mandibular arch (PA1), while rhombomeres 3-5 populate the hyoid arch (PA2), and cells from 5-7 fill the branchial arches (PA 4-7).

The first, or mandibular arch gives rise to the ventrally positioned bilateral Meckel's cartilages, which join at the midline and serve as the lower jaw in the larva, as well as the more dorsal palatoquadrates, which articulate with the posterior end of Meckel's to form the jaw joint (Mork & Crump, 2015). The pterygoid processes are anterior extensions of the palatoquadrate that contact the ethmoid plate (neurocranium but NCC derived), the most anterior part of the neurocranium, to form the larval upper jaw (Figure 1.5a). The second, or hyoid, arch also forms two large cartilages, the dorsal hyosymplectics and the ventral ceratohyals, with a smaller interhyal cartilage linking the two as part of the hyoid joint. The ceratohyals each contact the unpaired basihyal cartilage at the midline. The hyosymplectic, a fusion of the plate-like hyomandibula with the symplectic rod, is connected to the neurocranium via the anterior part of the otic cartilage and thereby secures the jaw skeleton to the rest of the head. Moving posteriorly, arches 3–7 produce paired ventrolateral rod-like ceratobranchial cartilages affixed to small hypobranchials, which in turn attach to unpaired basibranchials at the ventral midline (Mork & Crump, 2015). Unique to the

larval zebrafish viscerocranium, the fifth pair of ceratobranchial cartilages, form several ossified pharyngeal teeth. The larval viscerocranium also contains several directly ossifying bones, the most notable of which is the fan-shaped opercle bone which projects from the dorsal hyomandibula (Mork & Crump, 2015).

**Characterizing facial development in *cblC***

In this dissertation we will use zebrafish as a model to understand the cellular and molecular mechanisms underlying craniofacial phenotypes in *cblC* disorder. Literature and case studies were discussed in previous sections and results using murine models of *cblC* suggest that MMACHC is necessary for proper facial development. However, phenotypes in mice are dramatically more severe than what has been documented in humans. Based on these observations, we studied facial development at the cellular level using the hg13 allele (mutation in zebrafish *mmachc* gene).

## Chapter 2. Overarching goals

To identify and characterize developmental phenotypes caused by a germline mutation of *mmachc* zebrafish.

### HYPOTHESIS FOR SPECIFIC AIM 1: *MMACHC* IS REQUIRED FOR TYPICAL LARVAL SWIM BEHAVIOR.

We hypothesize that MMACHC has a role in early neurodevelopment and that neurodevelopmental phenotypes manifest as brain malformations resulting in abnormal locomotor response to a dark-light-dark paradigm.

### SPECIFIC AIM 1. DOES THE HG13 ZEBRAFISH ALLELE HAVE BEHAVIORAL NEURODEVELOPMENTAL PHENOTYPES?

Prior studies have reported severe brain malformations, such as exencephaly, in murine *Mmachc* models (Chern et al. 2020). However, the embryonic lethality of the model prevents further exploration into behavioral manifestations. My first aim is to investigate whether the loss Mmachc will cause behavioral abnormalities. We will characterize the behavioral phenotypes using ZebraBox technology.

a. Examine the swimming patterns of hg13 mutants and wildtype siblings in response to the Dark-Light-Dark behavioral assay to assess brain function integrity.
b. Identify subtypes of swimming in accordance with Kaleuff et al. (2013) zebrafish catalog of behaviors, to further delineate abnormalities in behavioral response.

**HYPOTHESIS FOR SPECIFIC AIM 2: B12 BINDING OF *MMACHC* IS DISPENSABLE FOR CRANIOFACIAL DEVELOPMENT.**

Based on the results by Quintana et al. (2014) showing that the knockdown of *MMACHC* causes craniofacial defects in the absence of metabolite dysfunction we hypothesize that facial development is B12 binding independent.

**SPECIFIC AIM 2. CHARACTERIZE THE FACIAL CELLULAR PHENOTYPES ASSOCIATED WITH MUTATION O*F MMACHC* IN ZEBRAFISH**

There is a subset of *cblC* individuals with craniofacial abnormalities. However, the mechanisms underlying these developmental malformations have not been fully elucidated. In addition, due to the earlier study (Quintana et al. 2014) we believe *MMACHC* is involved in craniofacial development, however independent of vitamin B12 binding.

a. Investigate craniofacial development in *mmachc* mutants using a collagen (alcian blue stain) marker to examine skeletal structures of the developing viscerocranium.
b. Investigate neural crest cell lineage to track destination of cells using developmental cell markers (*sox10, barx1, col2a1a*).
c. Prevent facial phenotypes in the hg13 allele with a cobalamin binding mutant.

## Chapter 3. Methods

All larvae were maintained according to guidelines from The University of Texas El Paso Institutional Animal Care and Use Committee (IACUC). Euthanasia was performed according to guidelines from the 2020 American Veterinary Medical Association and based on approved protocol 811869-5. All embryos were maintained in E3 media (embryo medium), a nutrient rich solution used to maintain a controlled environment for embryos, at 28$^{oC}$ with a 14/10 light: dark cycle consistent with the light: dark cycle of adults.

### GENOTYPING

Genotyping was performed using a PCR-based approach combined with restriction enzyme digest. DNA was obtained by excising a small piece of the developing tail and collected in individual PCR tubes. Sodium hydroxide (50 mM) was added to each sample and samples were heated for 5 minutes at 95$^{oC}$, cooled to 4$^{oC}$ for 10 min, and pH adjusted with 6 µL of 500 mM Tris, pH: 8.0 (Fisher Scientific). Samples were centrifuged for 10 min at 10,000×g. Lysate was used directly for PCR (2 µl). Primers were designed to amplify the region flanking the *mmachc* hg13 allele (Fwd: TACTGGTCTCCGAGGGACTG and Rev: CAGAGAGATGCAGGCAGACA. PstI (New England Biolabs) restriction enzyme digest was performed after amplification to identify carriers. Digestion was performed according to manufacturer's protocol. The hg13 allele abrogates PstI digestion and therefore, can be used to detect the genotype of interest.

### Methodology for specific aim 1

#### *Zebrabox Behavioral Analysis*

Behavioral analysis was performed using the ZebraBox (ViewPoint Behavioral Technology, Montreal, Canada). Protocol, optimization, and behavioral endpoints were adapted from published methods (Kalueff & Stewart, 2012). At 5 dpf larvae were individually placed into

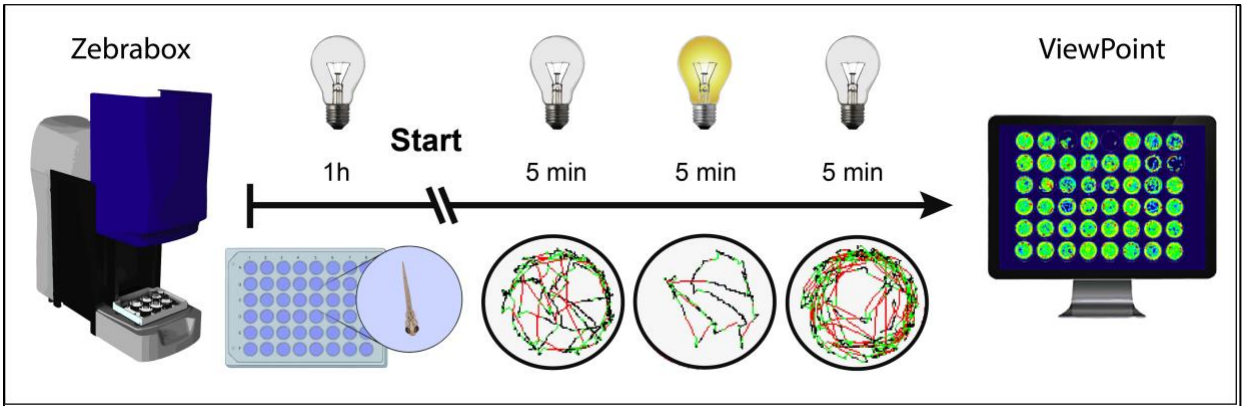


Figure 3.1 Dark Light Dark behavioral assay
The methodology for our D-L-D assay to determine brain function abnormalities. The total duration of the assay is 15 minutes. The ViewPoint program that accompanies the Zebrabox provides flexibility when modifying the behavioral design and behavioral measures.

a 48-well plate filled with 1,500 mL of embryo media. The behavioral assay was previously optimized for a total duration of 15-minutes with lighting changes at 5-minute intervals (Reyes-Nava et al., 2020).

All larvae were acclimated under dark conditions inside the Zebrabox chamber for 1 hour prior to data acquisition (Figure 3.1). Data was collected for a total of 15 minutes, with five-minute

Table 4. ZebraBox behavioral endpoints derived from ViewPoint Software.

| Zebrabox measurements | | | | | | |
|---|---|---|---|---|---|---|
| **Inactivity** | **Small count** | **Large count** | **Inactive distance** | **Small distance** | **Large distance** | **Inactive duration** |
| Inactivity count | Small movement count | Large movement count. | Total distance covered by the animal in inactivity | Total distance covered by the animal in small movement | Total distance covered by the animal in large movements | Total duration spent in inactivity |
| **Small duration** | **Large duration** | **Time** | **Distance** | **Speed** | **Movement** | • Time (s)<br>• Distance (mm)<br>• Speed (mm/s) |
| Total duration spent by the animal in small movement | Total duration spent by the animal in large movements | Total small duration and large duration | Total small distance and large distance | Distance/Time | Total small count and large count | |

intervals of dark, light, and dark transitions. The automated video recording reported the duration (s) and distance of swimming (mm) (Table 4). The swimming measures were broken up into small (4-8 mm/s) and large (>8 mm/s) (Figure 3.2). Experiments were performed in biological duplicates using a minimum of N= 30 larvae per trial. A total of 5 trials were performed at 5 dpf. Each trial consisted of approximately 240 larvae which were collected for DNA and lysed right after behavioral recording was performed. Afterward, each sample collected, was genotyped (n= 240) for mutants and siblings. The resulting numbers of hg13 is n=38 and sibling (n= 41), heterozygous carriers were not added into the final analysis. In short, out of the 240 samples only 79 were used for the current study.

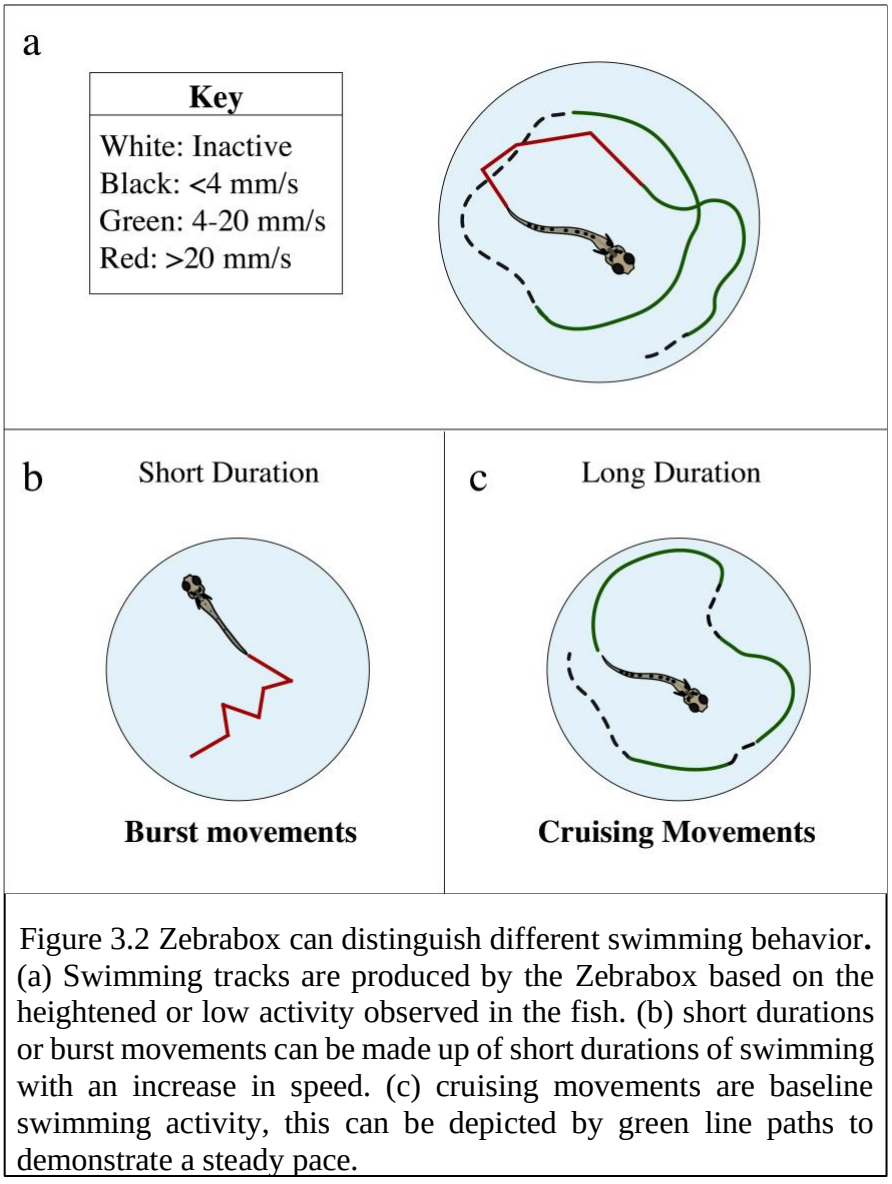


Figure 3.2 Zebrabox can distinguish different swimming behavior. (a) Swimming tracks are produced by the Zebrabox based on the heightened or low activity observed in the fish. (b) short durations or burst movements can be made up of short durations of swimming with an increase in speed. (c) cruising movements are baseline swimming activity, this can be depicted by green line paths to demonstrate a steady pace.

***Data Acquisition***

During data acquisition none of the genotypes are known. The raw data is provided in an excel sheet with a matching video file (avi). The initial recording of 5 minutes under dark conditions is used as a baseline measurement. This was followed by 5 minutes of lights on, followed by 5 minutes lights off. Speed was calculated by taking the average sum of distance divided by the average sum of time (mm/s). The fish was calculated as inactive if the movement fell below the threshold for movement (<4 mm/s) (Figure 3.2). Large and small movements were added to find the total movement. The same was performed to obtain total distance and total duration.

Table 5. Protocol settings for ViewPoint software.

| ViewPoint software settings | |
|---|---|
| **Experiment duration** | 15 minutes |
| **Integration time** | 300 s |
| **Color** | black |
| **Detection threshold** | 20-30 |
| **Small/large threshold** | 8 mm/s |
| **Inactive/ small threshold** | 4 mm/s |
| **Unit of length** | mm |

***Swimming tracks***

The ViewPoint software allowed for track tracing the larval movement. The total duration spent swimming could be further broken down into small and large durations (Table 4). Moreover, the program has colors assigned to the increases observed in speed (Figure 3.2a). Such as burst swimming which can be defined as small duration swimming or an increase in speed higher than 20 mm/s. In contrast you have coasting movements which are displayed as normal or typical swimming pace. The fish will show green tracks during swim recording if the speed is between 4-20 mm/s (Figure 3.2b).

***Manual observations***

Zebrabox AVI files were manually observed for abnormal behavior. These include complete inactivity, lack of a swim bladder, whirl pool like behavior, freezing, and general pattern (wall hugging behavior). All of the behavior analyzed was characterized as valid and defined using "Comprehensive Catalog of Zebrafish Behavior" (Kalueff et al., 2013).

***Automated calculations***

Bold or risk-taking behavior was measured by applying a center region of interest (ROI) as shown in Figure 3.3 (Axling et al., 2022; Kalueff & Stewart, 2012). Video recording software recorded the time larvae spent in the center ROI as a measure for bold behavior. The duration time of the center ROI was then averaged and subtracted from the total swim time within the entire ROI to use the remainder as a measurement for thigmotaxis (Basnet et al., 2019). The protocol was adapted and optimized using ViewPoint software (Kalueff & Stewart, 2012; Table 2). Regions of interest were adjusted to focus on the center so that the computer software could distinguish between the edges and the center space, adapting protocols to published work (Axling et al. 2022; Kalueff & Stewart, 2012).

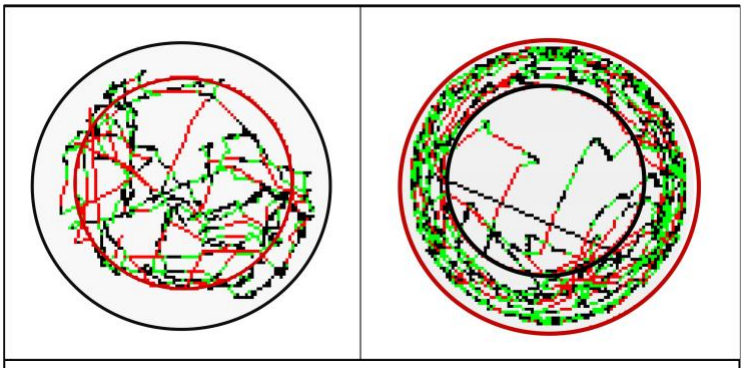

Figure 3.3. Swimming tracks with different ROIs
The left track shows a region of interest located at the center of the wells' boundaries (red circle). The track tracing to the right shows a region of interest at the edges of the well (red circle).

**Methodology for Specific Aim 2**

Data and Methods were published in Paz D*, Pinales BE*, Castellanos BS*, Perez I, Gil CB, Madrigal LJ, Reyes-Nava NG, Castro VL, Sloan JL, Quintana AM. Abnormal chondrocyte development in a zebrafish model of cblC syndrome restored by an MMACHC cobalamin binding mutant. Differentiation. 2023 May-Jun;131:74-81. doi: 10.1016/j.diff.2023.04.003. Epub 2023 May 5. PMID: 37167860. * Equal first author contribution.

***Genotyping of transgenic zebrafish expressing human MMACHC.***

The *Tg*(*ubi:MMACHC*) allele was produced using gateway cloning. The human MMACHC open reading frame, previously described (Quintana et al., 2014), was cloned into pME-MCS using BamHI and SacII cloning sites. An LR cloning reaction was then utilized to produce the *Tg*(*ubi:MMACHC*) in the pDestTol2CG2 backbone with p5e-Ubiquitin and p3ePolyA. Integration into the zebrafish host will produce a zebrafish ubiquitously expressing human MMACHC protein. The destination vector was injected at the single cell stage as described (Kwan et al., 2007) and genotyping was performed by detecting the human *MMACHC* open reading frame with primers (Fwd: ACTTACCGGGATGCTGTGAC and Rev: GGGTGTGGTAAAGGGAAGGT). For all experiments, embryos were obtained by natural spawning using adult *mmachc* hg13/+ Tg(*sox10:tagRFP*) carrying the hg13 allele, Tg(*ubi: MMACHC*) with or without the hg13 allele, or Tg(*col2a1a: EGFP*) carrying the hg13 allele.

***In vitro mRNA synthesis and microinjection***

Human *MMACHC* (RefSeq NM_015506.2) mRNA was produced using the T7 Ultra mMessage mMachine kit (Fisher Scientific) and a commercially available vector previously described (Quintana et al., 2014). The QuikChange Site Directed Mutagenesis kit (c.440G > A) (Fisher Scientific) was used to introduce a missense mutation into the open reading frame 39.

according to the manufacturer's instructions. Primers were as follows: Fwd: GAGAGAGCCTCCCAGAGCTACAGATAGAAATCATTGCTG and Rev: CAGCAATGATTTCTATCTGTAGCTCTGGGAGGCTCTCTC. According to a previously described empirical derivation, RNA was injected at a final concentration of 800 pg RNA/embryo at the single cell stage (Quintana et al., 2014). Larvae were kept in embryo medium at 28oC until 5 dpf, then fixed in 4% paraformaldehyde (Fisher Scientific) at room temperature for 1 hour before being stored in 1x PBS (Fisher Scientific).

***Microscopy***

As previously described (Quintana et al., 2014), alcian blue was conducted at 5 dpf. After dissection of the viscero- and neurocranium elements high resolution images were acquired with a Leica Laser Micro-dissection microscope at 40 and 63 magnifications. A 1 X 1 grid was used to obtain representative photos. Transgenic hg13 larvae (*mmachchg13/hg13* Tg*(col2a1a:EGFP*)) were staged and fixed with 4% paraformaldehyde (Fisher Scientific) at 5 dpf for confocal imaging. Larvae were dissected for genotyping, and the head tissue was unbiasedly imaged. The eyes were removed from the craniofacial region for mounting to image the hyosymplectic. Mutant and wildtype heads were tilted along a left or right ventrolateral axis and mounted in glass bottom dishes with 0.6% low-melt agarose (Fisher Scientific). Confocal imaging was carried out using a Zeiss LSM 700 at a magnification of 40x oil. Images were limited to the larval craniofacial region, namely the hyosymplectic region. A minimum of 8-20 z-slices were collected for each fish.

***Chondrocyte angle measurements***

Fiji, an open-source platform (Schindelin et al., 2012) was utilized to measure the angles between chondrocyte nuclei in the hyosymplectic region. Confocal microscopy was used to locate and capture regions of aberrant organization. We selected regions that were either 1) a cell with a

aberrant single nucleus relative to nearby cells or 2) disorganized nuclei (2 nuclei per cell) relative to neighboring cells using thorough image analysis. We assessed the angle between nuclei only in locations with aberrant chondrocyte organization to identify the degree of the disordered phenotype (quantitative measurement of penetrant phenotype). To acquire a quantitative estimate of the qualitative phenotype detected by microscopy, we compared the nuclear angle in these locations to the exact region in wildtype siblings. Concurrently, we counted the average number of surrounding cells in regions identified as having aberrant organization (Kimmel et al., 1998).

***Viscerocranium measurements***

Whole-morphology head angle measurements were performed (Staal et al., 2018). Quantification of angle variance in cartilage structures was examined to reveal any minor craniofacial anomalies. Angles were taken at numerous places using the Fiji open-source platform and compared to the average provided by wildtypes. The Meckel's-palatoquadrate (m-pq), ceratohyal (ch), Palatoquadrate-ceratohyal (pq-ch), and Meckel's (m) angles were all measured. In addition, the length of the Meckel's cartilage to the ceratohyal and the width between the palatoquadrates were measured (Quintana et al., 2017).

# Chapter 4 Behavioral characterization of the hg13 allele

## EXPLORING ABNORMAL BEHAVIOR ASSOCIATED WITH MUTATION OF MMACHC

The hg13 allele has been reported to have metabolic and ocular phenotypes, but neurodevelopmental behavioral phenotypes have yet to be studied in this model (Sloan et al., 2020). Patients have been shown to have severe neurodevelopmental phenotypes across case studies (Agarwal et al., 2021; Beauchamp et al., 2009; Chen et al., 2022; Frattini et al., 2010; Scalais et al., 2023; Trefz et al., 2016; Weisfeld-Adams et al., 2013) and *Mmachc* rodent studies have also shown extreme cases of brain malformities; yet it is impossible to observe behavioral phenotypes due to the embryonically lethal effects in mice (Chern et al., 2020). However, our hg13 allele mutant survives much longer (around 2-4 weeks) (Sloan et al. 2020). Thus, making us the first group to investigate behavioral phenotypes that occur due to mutation of *mmachc*.

### Mutation of *mmachc* does not affect the overall behavioral response to Dark-Light-Dark transition but does increase movement under light conditions

We conducted a Dark-Light-Dark assay (DLD) to test for neurodevelopmental abnormalities. In this assay, we acclimate the fish for 1 hour, followed by a 5-minute baseline recording in the dark. This is unique from an ocular motor test, which requires a much longer acclimation. A single 5-minute light stimulus is applied, and the test concludes with 5-minutes of lights off (Figure 3.1). This differs from an ocular motor test which requires several light-on stimuli and monitor the first 30 second response. We are monitoring the entirety of the 5-minute session. Thus, this test analyzes the behavioral response to lights on and off transitions and detects visible abnormalities using video recordings. Studies using this assay have reported typical V-pattern swimming responses in larval fish (Basnet et al., 2019).

The results of our D-L-D assay revealed a normal V-pattern for swimming distance for wildtype siblings and homozygous mutants when total distance was plotted (Figure 4.1). A significant increase in distance traveled by hg13 mutant larvae was observed during the 5-minute light phase, when compared to larvae to wildtype siblings (Figure 4.1). Moreover, an increase in the total duration of swimming was present in mutant animals during the light condition (Figure 4.1b). This was complemented by a significant increase in total movement count during the light condition (Figure 4.1d). Interestingly, the typical V-pattern of behavior was not present when addressing speed (total distance/time) (Figure 4.1c). This was attributed to a decrease in baseline speed relative to the sibling wildtype fish. The speed at which the mutants swam was significantly slower at baseline, although distance was normal.

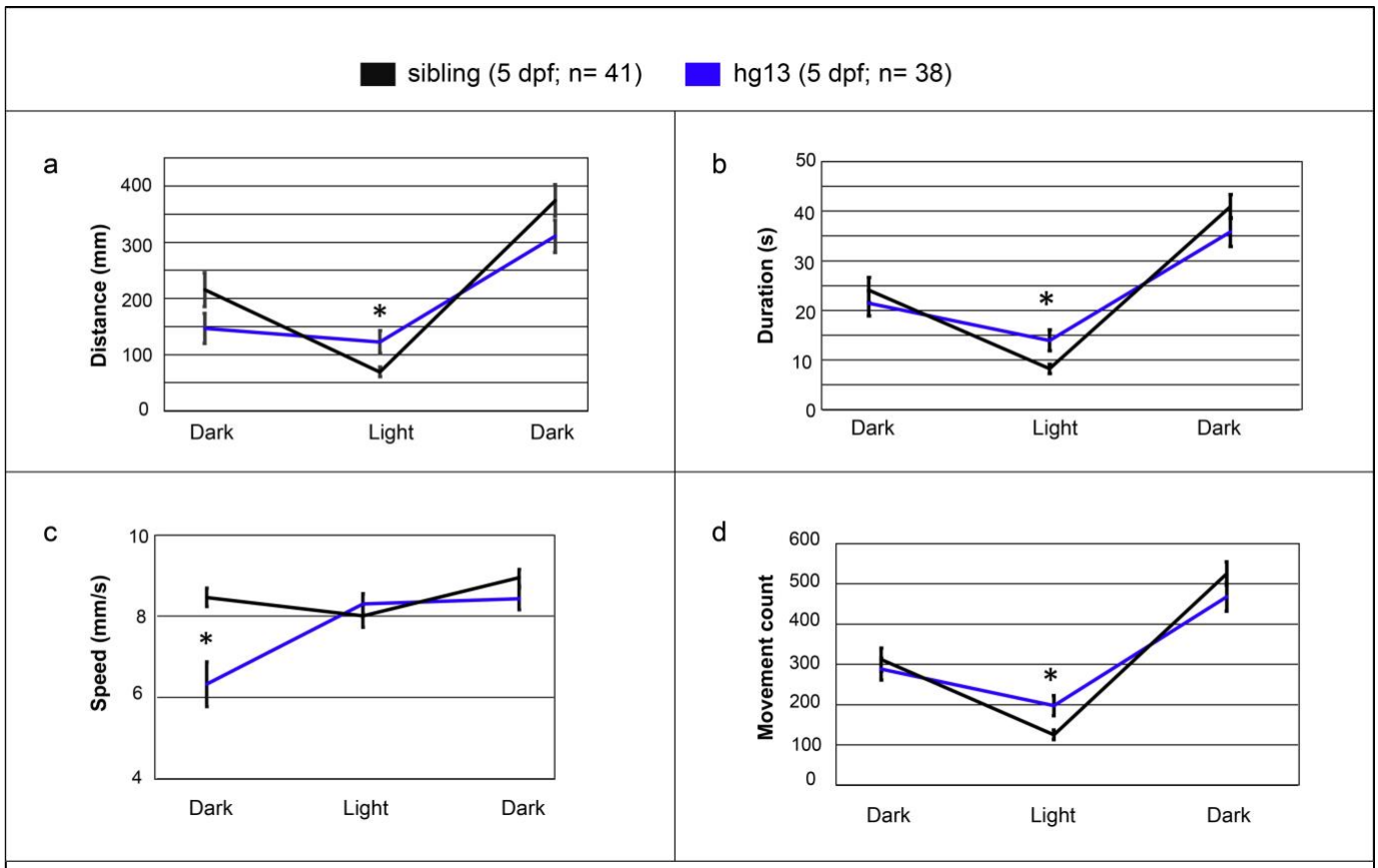


Figure 4.1 DLD assay results under dark, light, dark transitions.
The following graphs collectively show the behavioral patterns of the sibling and mutant zebrafish larvae under different transitions. (a) The distance shown depicts the typical V-pattern as described (Basnet et al., 2019). The same is seen in movement count (d) and duration (b). However, speed had shown a different response than what was anticipated.

**STAR PLOT ANALYSIS REVEALS LOCOMOTOR DIFFERENCES IN THE HG13 ALLELE.**

The ZebraBox provides a readout of multiple parameters. To get a broader sense of what was occurring during each timed interval, I created a radar graph, also known as a star plot, to provide a representation of all behavioral parameters (Figure 4.2). A total of 3 star-plots were created under each lighting conditions. Figure 4.2a depicts the baseline behavior of sibling and hg 13 mutant and shows that the sibling behavior completely overlaps the mutant behavior. The light green is represented as the sibling behavior. Total distance and movement of mutant larvae is modestly increased; however, no significance was identified between the two groups. Some of the numbers are too small to see such a drastic change including swimming speed.

The speed in baseline readings was significantly slower in hg13 mutants in comparison to the sibling. Decreases in movement and total distance can be observed by the overlapping (medium green) features sibling (light green) has on mutant fish (dark green). In Figure 4.2b the total time spent swimming in large and small movements was significant during the time spent with lights on. Based on the radar plot (Figure 4.2b) homozygous carriers of the hg13 allele had an increased number of small swim counts and increased numbers of large swim counts. This increase in counts in each behavior coincided with increased small distance travelled and increased large distance travelled.

However, overall speed was not dramatically different (Figure 4.2). Like the baseline conditions the same graph pattern is shown with sibling overlapping the behavior observed in mutants (Figure 4.2c). The biggest difference that can be observed when comparing the parameters of the baseline star plot is a reduction in inactivity. The inactivity duration and distance is nearly depleted in both mutant and sibling wildtype. This is consistent with what is reported in Basnet et

al. (2019). The expected increase in movement is anticipated once there is a transition from light to dark. Thus, the expected outcome shows normalcy in that transition (Figure 4.2c).

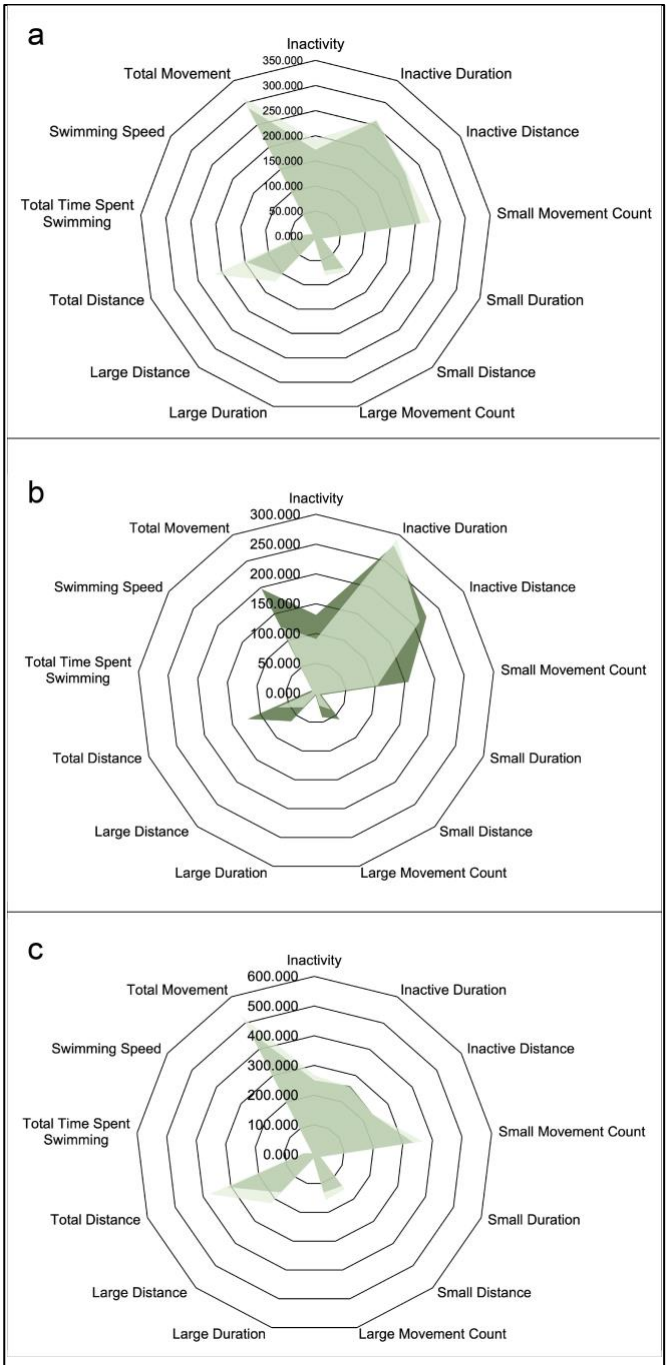


Figure 4.2. Star plots under different light intervals (a) Under baseline recording the mutant larvae behavior is completely overlapped by the sibling wildtype larvae. (b) under the light stimulus the larvae had shown a significant increase surpassing the sibling graph. (c) a complete overlap in behavior is observed again in the final dark reading. N=41 Sibling and N= 38 hg13.

**Distinguishing swimming behavior through analysis of small and large swimming bouts**

From the star plots we noted differences in the movements of the hg13 mutant larvae. In Figure 4.3b you can see an increase in small and large bouts of swimming time and distance in light conditions. To further investigate the behaviors that are observed, we then measured the two types of swimming behavior that are reported by the VisionPoint software as 'small' and 'large'. In Figure 4.3a the graph presents the time the animals spend in small versus large movements (refer to Figure 3.2 for key of measurements). In Figure 4.3b the differences in small and large swimming distances are compared. Homozygous mutants demonstrated a significant increase in both distances and time spent swimming in both large and small movements. *$p<0.05$. These data are consistent with our radar plot analysis which indicated increased distance and time spent in both conditions. Our radar plot indicated specific dramatic increases in small distance and large distance swam, but more mild increases in time spent making small and large movements in swimming behavior.

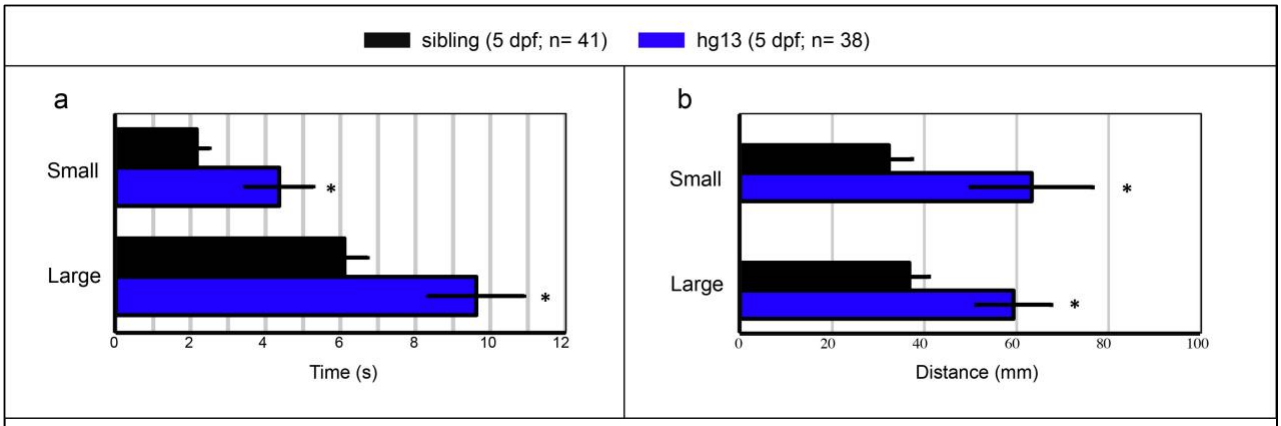


Figure 4.3 Small and large bouts of swimming
Comparison of time spent (a) and distance traveled (b) in small and large burst behaviors by sibling wildtype and homozygous mutants. *$p<0.05$.

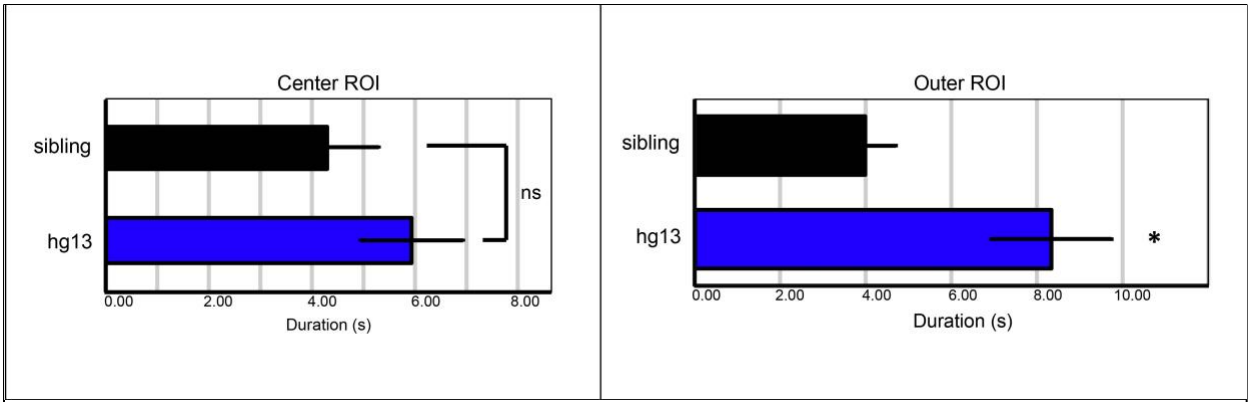


Figure 4.4 Thigmotaxis and bold behaviors.
(b) Time spent in the center ROI was not significant. (c) Time spent in the outer ROI was increased in the mutant fish. *p<0.05. N=41 Sibling and N= 38 hg13.

***Behavioral Trends of Zebrafish, Thigmotaxis, and Bold Behavior***

The ZebraBox exports TIF images of the swimming tracks recorded for the total duration of the behavioral test. These TIF images suggested can be utilized to set regions of interest (ROI), an important factor in testing for thigmotaxis or wall hugging behavior. In addition, the increases in activity during the light may be due to traits of 'boldness' or risk-taking behavior. Since reports have shown that anxiety one potential outcome associated with light stimulus, if there is a chance the fish are experiencing less anxiety than this could be attributed to bold behavior, otherwise

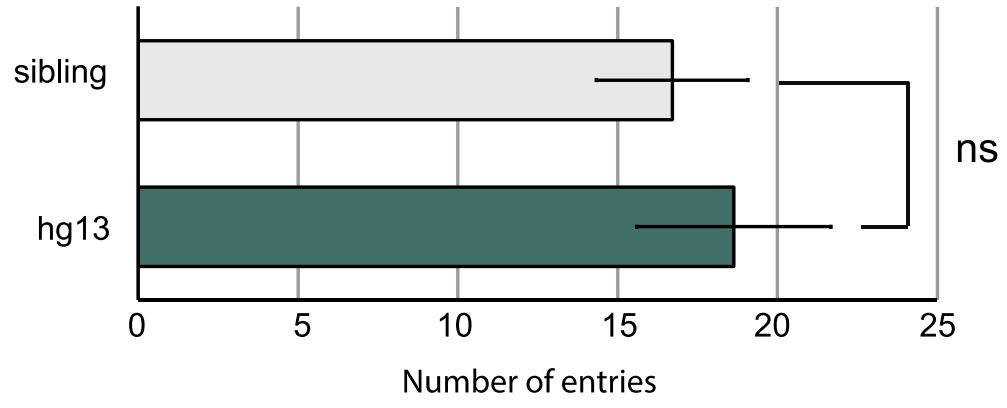


Figure 4.5 Number of entries into the center ROI
No significant differences were observed in the number of entries in the center ROI between sibling and hg13 mutant zebrafish. N=41 Sibling and N= 38 hg13.

known as risk taking as described and defined by Kalueff et al. (2013) behavioral catalog. For zebrafish behavior, thigmotaxis can be defined as "a preference for staying in close proximity to the edge/side and avoiding open/central areas". Bold or risk-taking behavior is defined as a zebrafish displaying increased exploratory behaviors, for example exploring the middle ROI at a higher rate (Kalueff et al., 2013). Thus, we set a middle ROI and an outer ROI, near the wall which would be more consistent with wall hugging behavior. We measured the time spent swimming in both the outer and center ROI between hg13 mutants and siblings (Figure 4.4). Significance was observed within the time spent in the outer ROI, showing a preference in the region, which can be attributed to the increased time spent in the region. Then we monitored the number of entries into the middle area (Figure 4.5). A higher number of entries would be associated with higher risk-taking behavior. The results revealed no significant difference between the frequency in movement into the center ROI among the two groups (Figure 4.5). Thus, mutant larvae did not display bold or risk-taking behavior significantly different than the wildtype. The percentage of time spent within the outer ROI and center ROI was also analyzed (Figure 4.6). We found that mutants spent more time in the outer regions and less in the center, indicated a preference for the wall hugging behavior despite having the same number of total entries into the middle region.

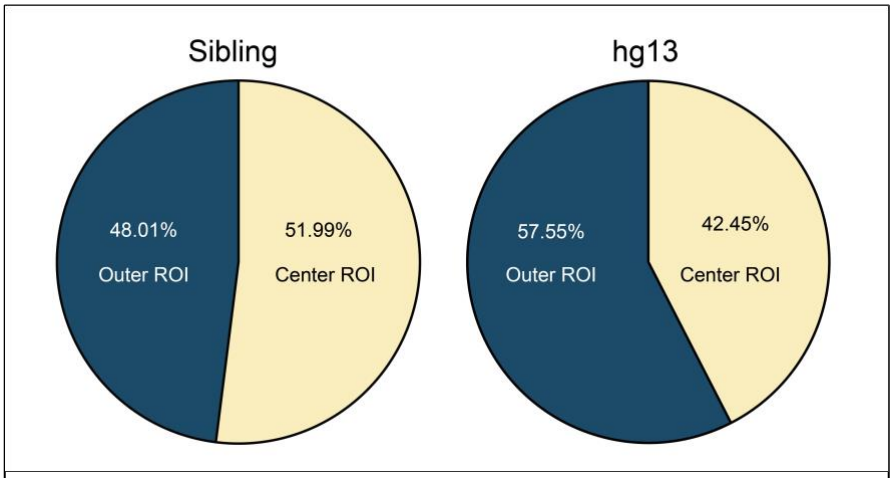


Figure 4.6 Percentage of time spent in ROI
Sibling pie graph shows a higher percentage of time spent in the outer and center ROI was nearly identical. Whereas the hg13 larvae show a preference for the outer ROI. N=41 Sibling and N= 38 hg13.

## Chapter 5. Characterizing craniofacial phenotypes associated with mutation of *mmachc*

Data and Methods were published in Paz D*, Pinales BE*, Castellanos BS*, Perez I, Gil CB, Madrigal LJ, Reyes-Nava NG, Castro VL, Sloan JL, Quintana AM. Abnormal chondrocyte development in a zebrafish model of *cblC* syndrome restored by an MMACHC cobalamin binding mutant. Differentiation. 2023 May-Jun;131:74-81. doi: 10.1016/j.diff.2023.04.003. Epub 2023 May 5. PMID: 37167860. * Equal first author contribution.

### MMACHC MUTANTS DO NOT SHOW OVERT MORPHOLOGICAL DEFECTS IN CRANIOFACIAL DEVELOPMENT.

Studies have shown that global deletion of *Mmachc* in mice causes cleft palate (Chern et al., 2020), but these phenotypes are not consistent with facial dysmorphia in patients, as they are more severe. Therefore, we sought to characterize craniofacial development in a germline mutant zebrafish (hg13 allele) of *mmachc*. The larvae were stained at 5 dpf with alcian blue. Since craniofacial phenotypes are mild to moderate in *cblC*, we sought quantitative measurements of facial development (Quintana et al., 2017). We measured the length from the ceratohyal to the tip of the Meckel's cartilage (m) and the width between the palatoquadrates (pq) using ImageJ measurement tools (Figure 5.1). Increases in width between each end of the palatoquadrates and at the extension of the Meckel's cartilage from the ceratohyal was quantified (Figure 5.1). Next, we measured the angles of several structures within the viscerocranium to determine the extent of these abnormalities (Staal et al., 2018). Using ImageJ software, we applied measurement tools to record the angles between the Meckel's cartilage: palatoquadrate: m-pq, the angle of the ceratohyal: ch, the palatoquadrate: ceratohyal angle: pq-ch, and angle of the Meckel's cartilage: m

in sibling wildtype and the hg13 allele (Figure 5.1). We did not detect any significant differences in the formation of these structures in mutant larvae.

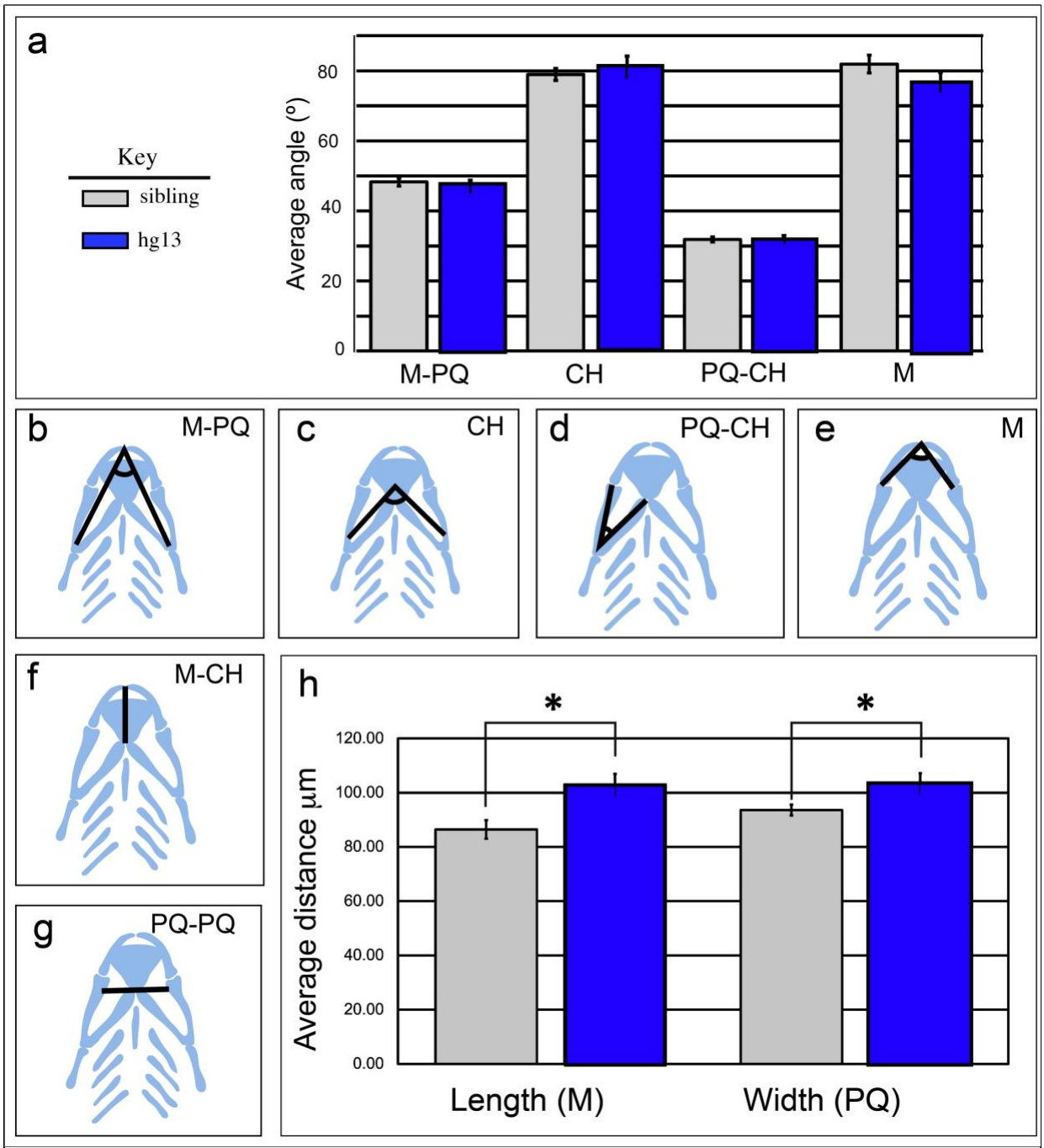


Figure 5.1 Craniofacial measurements using Alcian blue stain
(a) Average angle between measurements the indicated regions. (b) Distance and length measurements of the palatoquadrates. N= 41, hg13; N= 30 sibling

We next analyzed early neural crest development using the *Tg*(*sox10:tagRFP*) transgene (Figure 5.2) and in situ hybridization of *barx1* (Sperber and Dawid, 2007) at 30 hpf (RFP), 40 hpf (RFP), and 2 dpf (*barx1*) (Figure 5.3). We detected the pharyngeal arch shape and structure during early development. Pharyngeal arches are temporary structures whose cells produce cartilage and bone. No morphological deficits were observed in the shape of the pharyngeal arches at any stage or with either marker analyzed. We observed normal structures of the pharyngeal arches using the

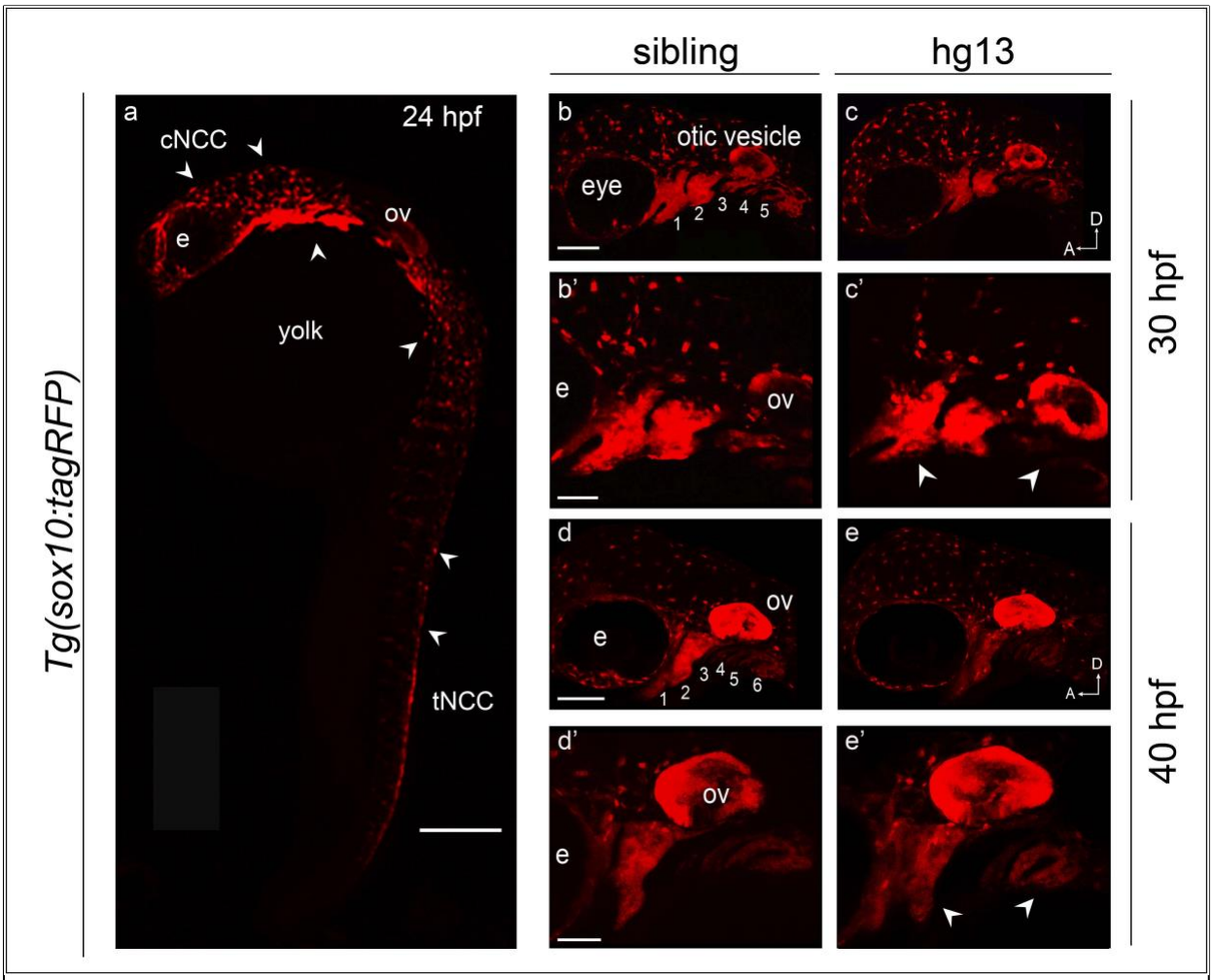


Figure 5.2 Comparison of pharyngeal arch structures in wildtype and mutant larvae (hg13). a-e are representations of mutant and sibling expression of RFP at 30 and 40 hours post fertilization (hpf). Example expression of RFP is shown in on the left panel at 24 hpf. Numbers indicate visible arch structures.

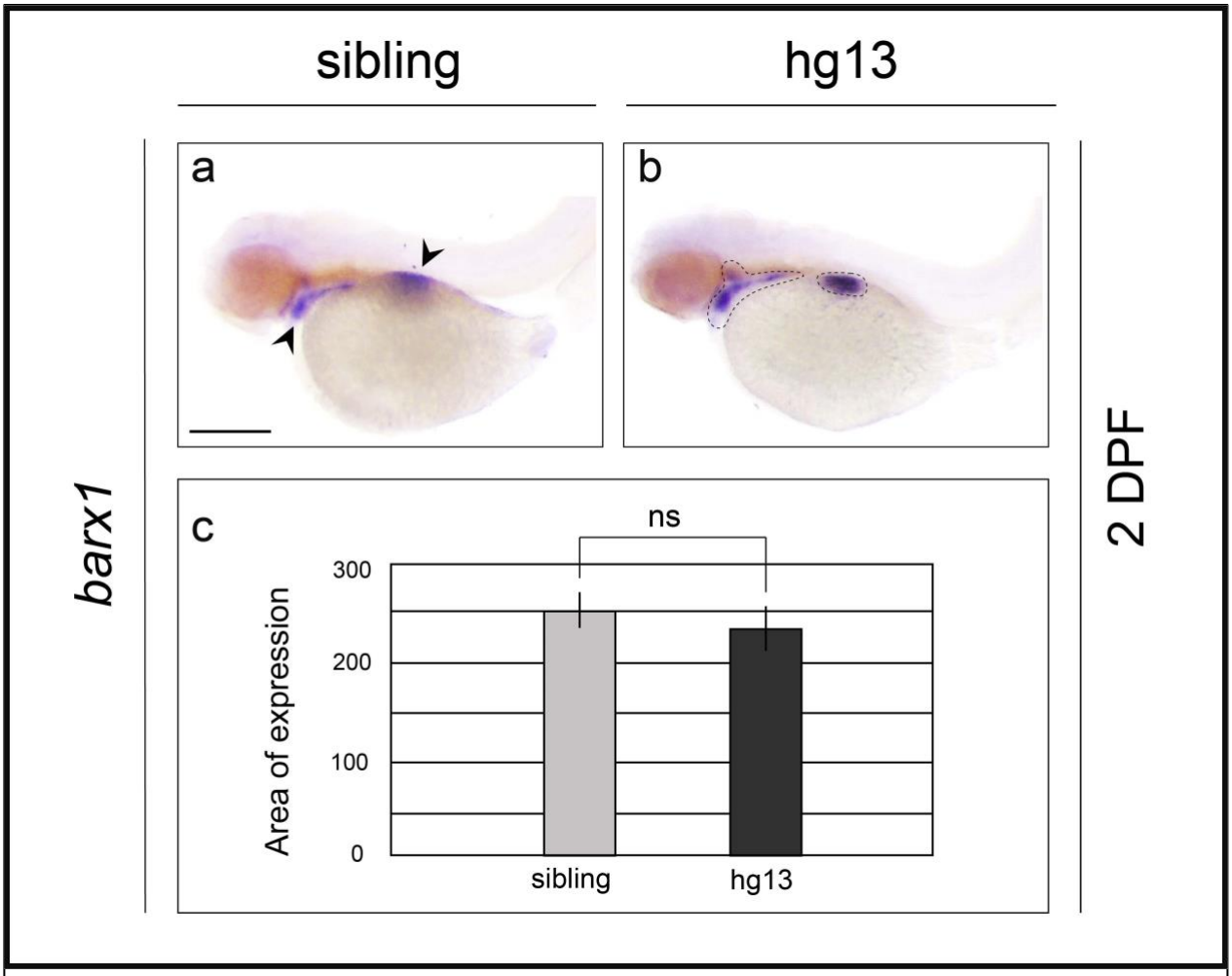


Figure 5.3 *In situ* hybridization of *barx1* in sibling and homozygous mutants (hg13). At 2 dpf *barx1* shows a normal expression. The purple indicates positive stain. The area of expression was quantified in the graph below. No significance was observed. Scale bar at 200 μm

*Tg*(*sox10:tagRFP*) at all time points analyzed (Figure 5.2). At 2 dpf we also monitored *barx1* expression. *barx1* is expressed in migrating NCCs. We observed normal location and level of expression of *barx1* in mutants (Figure 5.3).

**Mutation of *mmachc* is associated with abnormal chondrocyte organization.**

To investigate the subtle alterations of the extension of the Meckel's cartilage and width of the palatoquadrate, we performed alcian blue staining at 5 dpf and performed high resolution imaging of the pterygoid process of palatoquadrate (Figure 5.4). Chondrocytes within the

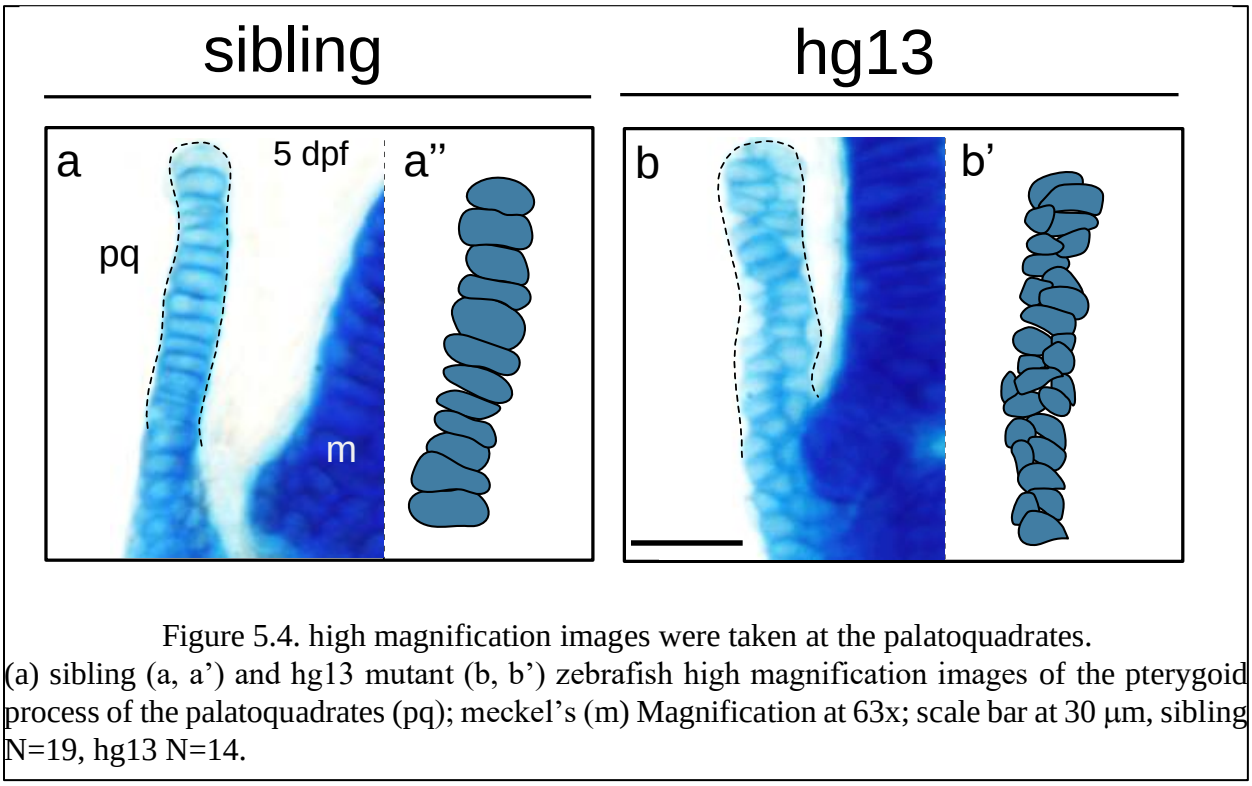


Figure 5.4. high magnification images were taken at the palatoquadrates.
(a) sibling (a, a') and hg13 mutant (b, b') zebrafish high magnification images of the pterygoid process of the palatoquadrates (pq); meckel's (m) Magnification at 63x; scale bar at 30 μm, sibling N=19, hg13 N=14.

pterygoid process of palatoquadrate were organized adjacent to one another (penny like stacking) in wildtype siblings but chondrocytes from homozygous mutant larvae displayed an abnormal pattern of organization. We further characterized these deficits in chondrocyte development using the *Tg*(*col2a1a:EGFP*) transgene. High resolution confocal microscopy demonstrated normal chondrocyte organization in wildtype clutch mates at 3, 4, and 5 dpf. In contrast, we noted abnormal organization of chondrocyte nuclei in the ventral end of the hyosymplectic at 4 dpf in homozygous mutants (Figure 5.5e). We observed cells with multiple nuclei and cells with a single nucleus, whereby the single nucleus was not in alignment to the nucleus of an adjacent cell (Figure 5.5f). We sought to quantify the severity of this nuclear disorganization and therefore measured the angle between nuclei within the regions where mutation of *mmachc* is associated with abnormal chondrocyte organization. As shown in Figure 5.6, we measured all potential angles between the nuclei of neighboring cells. We compared that angle to the average angle of nuclei in the same region in wildtype siblings. We found that the average angle between nuclei in the mutant

larvae, within targeted regions, was significantly reduced relative to wildtype siblings (Figure 5.5g, $p < 0.05$). Since some cells had multiple nuclei, which altered the number of nuclear angles per region, we next measured the number of cell contacts between neighboring cells (Figure 5.6b). We found that homozygous mutants had on average approximately 2.5 neighboring cells while siblings averaged 2.2 neighboring cells (Figure 5.5h right panel). This result was statistically significant ($*p < 0.05$).

**CHONDROCYTE ORGANIZATION CAN BE RESTORED USING PATIENT DERIVED VARIANT CBL BINDING MUTANT.**

We designed a restoration experiment whereby we injected mRNA encoding either the wildtype human MMACHC protein or a human MMACHC mRNA encoding the patient derived

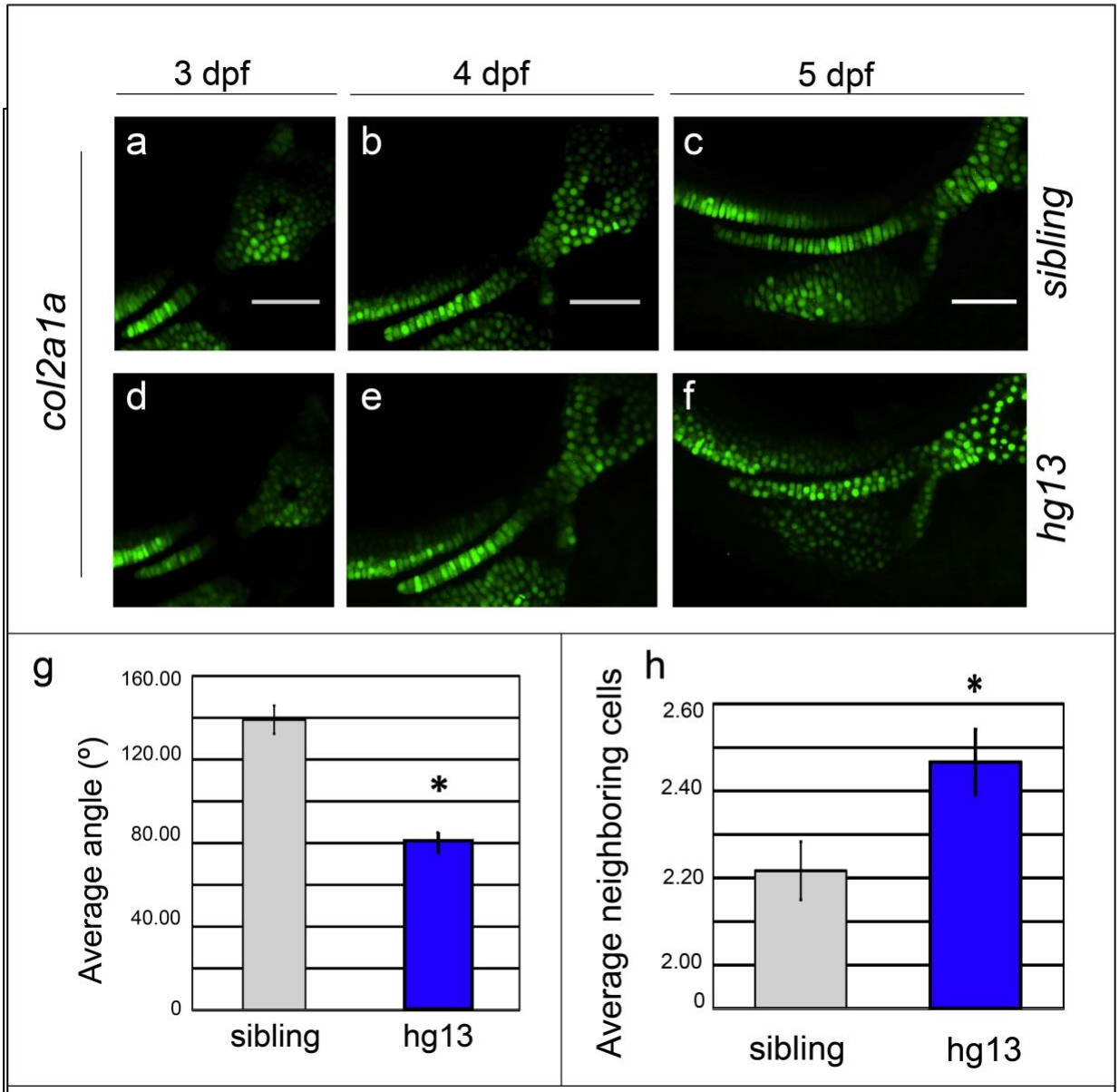


Figure 5.5. High-resolution images of chondrocytes in the hyosymplectic.
(a) Chondrocytes were imaged in sibling and homozygous mutants (hg13) at 3, 4, and 5 dpf. (b) the average angle between nuclei was measured at 5 dpf. In the adjacent graph, the average of neighboring cells was quantified at 5 dpf. Both measurements were observed in the hyosymplectic. $p<0.05$. hg13 N = 30; sibling N = 30. Magnification at 20×; scale bar at 20 μm.

variant, p.Gly147Asp. The p.Gly147Asp variant is in the cobalamin binding domain of MMACHC and is conserved in the zebrafish. Previous studies have demonstrated that this variant completely abolishes the ability of MMACHC to bind to both cyanocobalamin and hydroxycobalamin,

eliminating enzymatic activity, and resulting in early onset cobalamin deficits. We injected RNA encoding the two mRNAs into hg13 mutants and their clutch mates and subsequently analyzed chondrocyte organization at 5 dpf. We observed abnormal chondrocyte organization in the non-injected hg13 homozygous larvae within the hyosymplectic region (Figure 5.7) This was associated with a decreased angle between nuclei consistent with data in (Figure 5.7a, $p < 0.05$). Injection of wildtype human *MMACHC* encoding mRNA (Figure 5.7) substantially improved chondrocyte organization and the nuclear angle after injection was significantly improved relative to non-injected siblings (Figure 5.7a $p < 0.05$), although it did not result in a complete restoration of the penny-like stacking observed in wildtype siblings as observed by confocal microscopy (Figure 5.7b). Intriguingly, the injection of *MMACHC* p.Gly147Asp encoding mRNA into hg13 homozygous embryos restored the angles between nuclei (Figure 5.7a). The degree or restoration was nearly equivalent to that observed after injection of wildtype *MMACHC* mRNA (Figure 5.7a). The angle in those animals injected with wildtype *MMACHC* or the p.Gly147Asp variant were not statistically different than non-injected controls or with one another, indicating equivalent restoration by both mRNAs. While the angle of nuclei was restored, we noted from imaging that the restoration of overall chondrocyte development (Figure 5.7b) was only a partial restoration (cells appeared larger and still packed together in some regions). Despite the partial nature of the restoration, we also observed restoration when analyzing the average number of neighboring cell contacts. The injection of wildtype *MMACHC* mRNA and the *MMACHC* p.Gly147Asp encoding mRNA restored the number of neighboring cell contacts (Figure 5.7b). We performed additional restoration of the hg13 chondrocyte phenotype using the *Tg*(*ubi:MMACHC*) allele (ute2tg), which

expresses wildtype human MMACHC under the control of the ubiquitin promoter (Figure 5.8). This assay served as a control experiment with which to test the specificity of the restoration and phenotype from mRNA injection. The ubiquitous expression of wildtype MMACHC completely

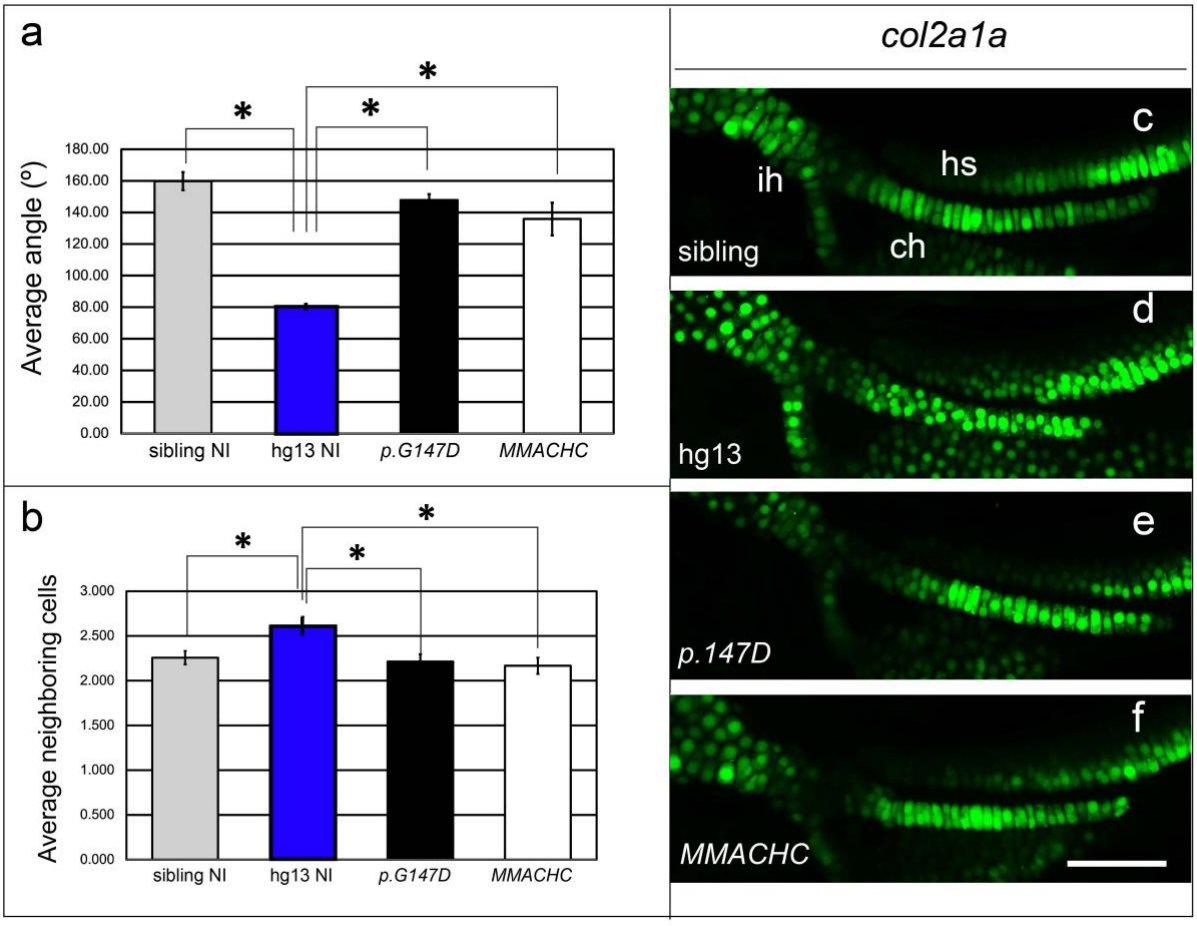


Figure 5.7 Restoration of chondrocytes

(a) The average angle between nuclei and the average number of neighboring cells (lower graph) were quantified in sibling wildtype (no mRNA injection), homozygous mutants (hg13 NI, no mRNA injection), homozygous mutants injected with p.G147D or those injected with wildtype MMACHC encoding mRNA. (b) Chondrocyte development in the hyosymplectic was imaged in each group described in (a) using the *Tg(col2a1a: EGFP)* transgene. * indicates a $p < 0.05$. sibling, N = 7; non-injected hg13, N = 7; MMACHC$^{p.Gly147Asp}$, hg13 N = 7; MMACHC, hg13 N = 5. Magnification at 40×; scale bar at 50 μM

restored the angles between nuclei (Figure 5.8a; $p < 0.05$) and the average number of neighboring cell contact (Figure 5.8b).

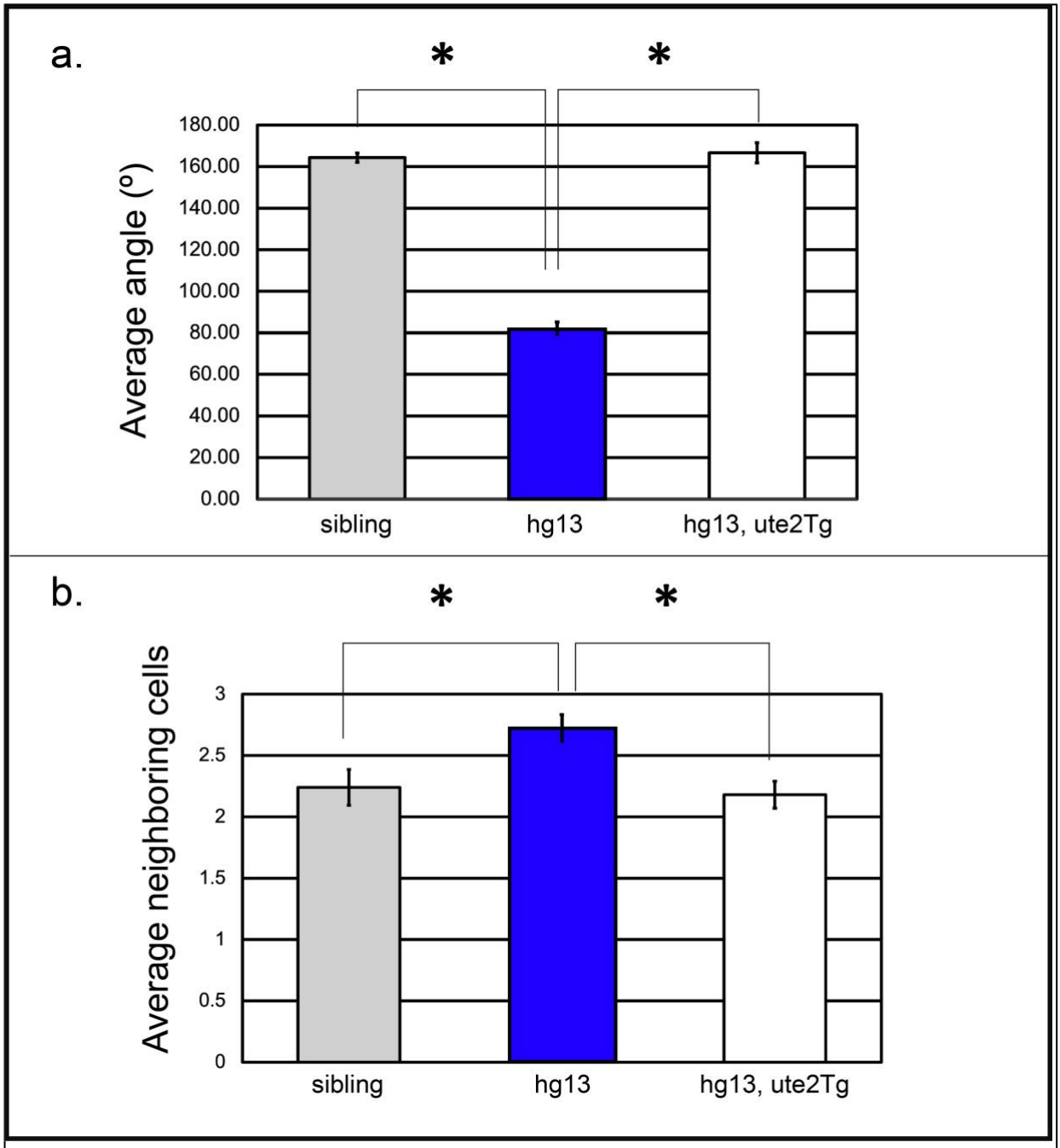


Figure 5.8 Chondrocyte and nuclei stacking was restored.
Additional restoration of hg13 chondrocytes were performed using wildtype human MMACHC. (a) The angle average among nuclei was restored and (b) the neighboring nuclei had less than 3 neighbors making the numbers significant. N= 5 sibling; N=5 hg13; N=6 hg13, ute2Tg. * Indicates a $p < 0.05$

# Chapter 6. Discussion

*cblC* syndrome is a multifaceted disorder that is most severe in its early onset form. Patients diagnosed with *cblC* are unable to metabolize vitamin B12 causing a wide range of developmental abnormalities that can be lethal. The phenotypic manifestations linked to *cblC* syndrome exhibit a lack of specificity and a wide range of severity, thereby posing a challenge in understanding the underlying mechanism responsible for the extensive disruption observed. Investigating molecular pathways associated with a pathogenic gene can support the evidence of its causal role in disease, while also offering valuable insights that could inform the development of therapeutic interventions. Because the exact pathophysiology of *cblC* and the role of *MMACHC* in processes outside of metabolism remains unknown, the goal of this dissertation was to investigate its role in craniofacial development and neurodevelopment.

## DOES THE HG13 MUTANT ZEBRAFISH DEMONSTRATE ANY BEHAVIORAL ABNORMALITIES?

At 5 dpf, larval zebrafish with the hg13 mutation exhibited increased locomotor activity when exposed to changes in light conditions, specifically transitioning from dark to light. I conducted a comprehensive analysis of behavioral abnormalities by employing both manual observations and a high-throughput automated tracking system to closely monitor the behavior of larvae. The fish were carefully placed within a multi-well plate, inside a closed chamber and were acclimated in the dark for an hour, followed by 5 minutes light on and another 5 minutes in dark conditions. The setup and software were optimized and published prior to testing. During the recordings conducted under light conditions, mutant zebrafish exhibited a notable elevation in their locomotor activity as a response. Studies have shown that larvae reduce distance swam when transitioned from dark to light conditions as demonstrated by Basnet et al. (2019).

Here we report that the hg13 mutant larvae did respond to the dark to light transition, as this can be seen in the slight decrease in activity that gives the V-pattern; however, it is important to note that the mutant zebrafish larvae do not exhibit the same response as the wild type. Instead, the hg13 mutants exhibit elevated levels of activity in terms of distance swam, duration spent swimming, and movement counts.

Locomotor activity in zebrafish is a complex behavior produced by evolutionarily conserved pathways among vertebrates. In the dark-light-dark behavioral assay, zebrafish larvae demonstrate a clear and concise pattern of movement depending on the different transitions in light (Basnet et al., 2019). Due to the behavioral assays' validity, it is commonly employed in the screening of neuroactive drugs (Basnet et al., 2019). It has been shown that the dark to light transitions show a decrease in locomotor activity in larvae, whereas the light to dark shows an increase in behavioral activity (Basnet et al., 2019). As shown in the results, the hg13 allele mutants displayed the expected V-pattern during the dark-light-dark assay according to distance traveled. However, at the light stimulus the mutants demonstrate hypermobility relative to wildtype siblings. These locomotor responses are dependent on the brain's integrity, nervous system development, and visual pathways (Basnet et al., 2019). For example, the use of convulsant drugs has shown dose dependent responses towards the light dark transitions. At low concentrations they increased locomotion in the dark, as should, however, in high concentrations a reversal in behavior was observed, i.e., at the transition of dark to light there was an increase and from light to dark there was a decrease in movement.

To further assess what was occurring during the surge of activity at the light stimulus, I analyzed small and large bouts of movement, or as mentioned, burst and coasting behavior. Both types of movement had shown an increase upon the light stimulus. Nonetheless, the results

collectively provide a reason to further investigate earlier developmental timepoints to address neurodevelopmental concerns.

**Mutant zebrafish do not show enhanced risk behavior**

Thigmotaxis is the tendency of an animal to move in contact with a vertical surface. In thigmotaxis, an animal moves away from the center of an arena and toward the edge or perimeter of an unfamiliar environment, such as a wall. As a result, it is sometimes referred to as wall-hugging behavior. It is a reliable indicator of anxiety and has been found to be maintained across species such as fish, rats, and humans. Thigmotaxis causes zebrafish larvae to gravitate toward the walls of the multi-well plates, a behavior that can be seen as early as 5 dpf. Anxiolytic medications like diazepam and anxiogenic drugs like coffee have both been demonstrated to affect thigmotaxis in larval zebrafish. As a result, thigmotaxis is critical in the research of anxiogenic and anxiolytic medicines.

We tested wall hugging behavior because hyperactivity in light can be the result of higher risk-taking behavior or lack of fear to light. Consequently, we specified a middle region and an outer region under the hypothesis that the hyperactivity was due to increased risk-taking behavior. We did not observe wall hugging behavior to be abnormal in mutant larvae, but the duration of the time spent swimming near the edges of the well were significant. Likely due to an increase in overall distance swam. But the number of entries to the middle was not different and therefore, we conclude that risk taking behavior is not increased in the mutant. Pharmacological interventions can lend more insight as to what this behavior may show us, particularly to test anxiety like behavior to light or a lack of anxiety like behavior. Nonetheless, larvae did not show a preference for swimming at the center ROI, using the distance and time spent within the ROI, however

additional quantitative analysis will lend more insight (Axling et al., 2022; Kalueff & Stewart, 2012).

**NEXT DIRECTION**

Future questions that come to mind are: What is the root cause of this behavior? Can this be a locomotive defect? A defect in visual response? Can this be an abnormal startle response? Can we determine the onset of neurodevelopmental abnormalities that could explain the behavior? Can we rescue this phenotype? To best answer this, some things need to be clarified.

The DLD test is customary to study neurodevelopment, which includes eye development in vertebrates. However, it can be influenced by locomotor defects. Under dark baseline conditions swim speed was reduced, suggesting that overall swim speed may be lower at baseline. An ocular motor test can be implemented to increase the rigor of our study. For example, a minute-by-minute analysis of light stimulus. Larvae would be expected to increase only in the first minute of light if the phenotype is ocular motor. On the other hand, if the response is sustained across all 5 minutes of the test, additional conclusions can be developed regarding brain development rather than a motor response. However, since most behavioral tests rely on motor movement in fish and assessing swim speed, it could be important to study a startle response in which early-stage larvae are prompted with an insect needle for movement.

Additional studies are underway currently to assess overall brain development. Abnormal development/morphology of the brain consistent with *cblC* could indicate the DLD response is attributed to abnormal brain development. Preliminary analysis at 2 dpf has shown reduced Elavl3 expression in forebrain, midbrain, and hindbrain. Elavl3 is an RNA binding protein present in neurons and therefore is a pan-neuronal marker. Sloan et al. 2020 reported *mmachc* mutant retinas were histologically normal during the embryonic period but developed pathological changes at the

end of the larval stage. Thus, it is likely that larvae can visualize the light and the deficits we observe behaviorally are a consequence of neural developmental defects.

Since larvae exhibited hypermotility in response to light, there are several interpretations. First, it could be the result of loss of vision. Yet vision is not affected until later stages. Second, it could be a motor deficit, but according to distance swam and star plot analysis, larvae behaved virtually the same overall and with a V-like pattern. Lastly, larvae could have more risk-taking behavior and not have an appropriate fear response to light. I performed a thigmotaxis measurement to better understand what was occurring in the phase of light stimuli by measuring two types of behavior as reported and defined in Kaleuff et al. (2013). I established a boundary to assess whether this was due to a fear/anxiety-like response. The area of this region was determined by the diameter of the well, as reported by Axling et al. (2022). Given the presence of two distinct regions of interest, I conducted a thorough assessment to determine the duration of time swimming within the inner circle, the number of entries, and the percentage time spent in each region. We found that mutant larvae had more time spent in both regions, consistent with the increased movement relative to wildtype. Mutant larvae did not have an increased number of entries into the middle but did show a slightly different overall percentage of time within each region. The measurement of time spent in the outer region serves as an indicator of wall- hugging behavior.

For future direction, a minute-by-minute analysis can provide more insight as to how the mutant fish are responding to the light stimulus. This would help us understand whether this hyperactivity is seen throughout the five minutes or if this is an immediate response that later attenuates over time. Seizure like behavior has been demonstrated if the initial minute of analysis is the only timeframe with enhanced motility. In addition, we could also assess the correlation of the hypermotility, or time spent in each region in response to the light.

So, what is next? We know *cblC* syndrome patients of early onset present very severe neurodevelopmental deficits. More commonly observed were brain malformations. Knowing there is a behavioral change, analyzing neurodevelopmental defects is essential. Investigating neurogenesis or neural connectivity during development is a good future direction of these data. If there are abnormalities in the development of neuronal cells this could be a starting point for behavioral deficits. If not, then we could speculate that there are other reasons for these behavioral abnormalities, for example muscle development could be an avenue of future exploration. Additional avenues may include studies on myelination and oligodendrocyte regulation.

Literature has reported several cases of brain malformations observed in the early onset form of *cblC* patients (Agarwal et al., 2021; Chen et al., 2022; Enns et al., 1999; Frattini et al., 2010). However, these cases are quite severe in that the patients present intellectual disabilities or severe developmental delays. These devastating phenotypes overshadow other neuropsychiatric endophenotypes that have yet to be explored. The following results are the first of its kind using a viable model organism to study the function of MMACHC in behavior. We are the first lab to explore behavioral abnormalities in a loss of function *mmachc* zebrafish model, something that is currently impossible in the mammalian model, due to embryonic lethality. Rodent models have proven that MMACHC may have a significant role in various tissues, including neurodevelopmental, but the model cannot live past a date where behavioral changes can be explored.

Case studies have shown that even treatment with Cbl derivatives brain abnormalities remain present, which is an indication that earlier time points of neurodevelopment are being affected. Brain abnormalities have been a common phenotype seen in patients. Light sheet microscopy and the use of Imaris volumetric analysis can be utilized in sibling and hg13 mutant

larvae to investigate whether brain structure is affected. Delays in white matter tracts have been reported in patients (Frattini et al., 2010). Using a myelin marker, we can visualize whether there is a defect among the hg13 allele. Since the buildup of toxic metabolites are occurring as the fish age, one can imagine that there will be a defect in lipid and neurotransmitter production. Therefore, limiting oneself to studying earlier time points will provide the foundation for the reason of such developmental defect.

**MUTATION OF MMACHC IN HUMANS CAUSES ATYPICAL FACIAL DEVELOPMENT.**

The mechanisms by which MMACHC expression regulates facial development are not entirely characterized. Mild to moderate facial dysmorphia has been observed in a subset of patients with *cblC* but these phenotypes are not well characterized in humans, are not completely penetrant, and can be subtle in nature. Here we characterized the cellular phenotypes associated with mutation of zebrafish *mmachc*. We questioned whether MMACHC cobalamin binding activity is required for proper facial development. Interestingly, we restored facial phenotypes in the hg13 allele through expression of a cobalamin binding mutant known to cause *cblC*. Collectively, these data implicate MMACHC in the regulation of craniofacial development and suggest that a domain outside of the MMACHC cobalamin binding domain is required for facial development. We observed nearly normal morphology of cartilage structures in the hg13 allele, but we identified a highly penetrant defect in chondrocyte organization in the pterygoid process of the palatoquadrate and the hyosymplectic. The shape and structure of pharyngeal arches was also relatively normal during early development. However, future experiments analyzing the endogenous expression of *sox10* or higher resolution images of *barx1* condensates could reveal mild abnormalities in mutant animals.

Our investigation revealed no substantial morphological anomalies in the development of major viscerocranium structures. These findings are consistent with the mild to moderate characteristics seen in *cblC* patients. Cerone and colleagues (1999) identified moderate traits such as a long face, a high forehead, large-low set ears, and a flat philtrum. The data gained from the hg13 allele and human patients contrasts with the abnormalities reported in *cblC* mice models, which are substantially more severe, including facial clefting (Chern et al., 2020).

We carried out a restoration experiment in which we injected mRNA encoding the patient-derived p.Gly147Asp variant. The p.Gly147Asp variation is found in the cobalamin binding domain (amino acids 122-156) and prevents binding to hydroxycobalamin or cyanocobalamin, causing cobalamin metabolism to be disrupted. According to quantitative assessments, the expression of the p.Gly147Asp expressing mRNA partially restored chondrocyte organization, indicating that cobalamin binding was not needed for normal chondrocyte development. More research is being performed into the ability of missense mutations in the other domains of MMACHC. Based on our results, we hypothesize that the mild to moderate facial phenotypes seen in persons with the hg13 allele are most likely the result of an unknown, but cobalamin-independent function. However, additional variants need to be tested. In summary, we offer a comprehensive phenotypic characterization of the zebrafish hg13 allele. Our findings will help to shed insight on the function of MMACHC in brain and facial development.

**FINAL THOUGHTS**

Mutations in MMACHC cause cblC disorder, which is a multi-system syndrome. To this point, mouse models are embryonically lethal and have limited our capacity to characterize specific phenotypes at the cellular and molecular level. In 2020, a zebrafish germline mutant was created to mimic *cblC* syndrome but was not completely phenotypically characterized. The mutant

exhibited metabolic syndrome and abnormal eye development. However, *cblC* has neurodevelopment, neuropsychiatric, facial, hematological, and many other phenotypes. We sought out to characterize additional phenotypes to provide construct validity towards the use of this zebrafish model for future studies. We identified behavioral phenotypes consistent with abnormal brain development and cellular facial phenotypes consistent with phenotypes present in patients. Thus, our work suggests that the hg13 allele is an appropriate model to characterize the role of MMACHC in brain and facial development.

## References


Adamson, K. I., Sheridan, E., & Grierson, A. J. (2018). Use of zebrafish models to investigate rare human disease. *Journal of Medical Genetics*, *55*(10), 641–649. https://doi.org/10.1136/jmedgenet-2018-105358

Ahrens-Nicklas, R. C., Whitaker, A. M., Kaplan, P., Cuddapah, S., Burfield, J., Blair, J., Brochi, L., Yudkoff, M., & Ficicioglu, C. (2017). Efficacy of early treatment in patients with cobalamin C disease identified by newborn screening: A 16-year experience. *Genetics in Medicine*, *19*(8), 926–935. https://doi.org/10.1038/gim.2016.214

Agarwal, A., Upadhyay, V., Gupta, A., Garg, A., Vishnu, V., Rajan, R., Singh, M., Bhatia, R., & Padma Srivastava, M. (2021). Cobalamin c disease: Cognitive dysfunction, spastic ataxic paraparesis, and cerebral white matter hyperintensities in a genetic but easily treatable cause! *Annals of Indian Academy of Neurology*, *24*(6), 997. https://doi.org/10.4103/aian.AIAN_729_20

Audira, G., Sampurna, B., Juniardi, S., Liang, S.-T., Lai, Y.-H., & Hsiao, C.-D. (2018). A Versatile Setup for Measuring Multiple Behavior Endpoints in Zebrafish. *Inventions*, *3*(4), 75. https://doi.org/10.3390/inventions3040075

Axling, J., Jakobsson, H., Frymus, N., Thörnqvist, P.-O., Petersson, E., & Winberg, S. (2022). Boldness in Zebrafish Larvae—Development and Differences between a Domesticated Lab Strain and Offspring of Wild-Caught Fish. *Fishes*, *7*(4), 197. https://doi.org/10.3390/fishes7040197

Basnet, R., Zizioli, D., Taweedet, S., Finazzi, D., & Memo, M. (2019). Zebrafish Larvae as a Behavioral Model in Neuropharmacology. *Biomedicines*, *7*(1), 23. https://doi.org/10.3390/biomedicines7010023

Beauchamp, M. H., Anderson, V., & Boneh, A. (2009). Cognitive and social profiles in two patients with cobalamin C disease. *Journal of Inherited Metabolic Disease*, *32*(S1), 327–334. https://doi.org/10.1007/s10545-009-1284-8

Breuer, M., & Patten, S. A. (2020). A Great Catch for Investigating Inborn Errors of Metabolism—Insights Obtained from Zebrafish. *Biomolecules*, *10*(9), 1352. https://doi.org/10.3390/biom10091352

Cerone, R., Schiaffino, M. C., Caruso, U., Lupino, S., & Gatti, R. (1999). Minor facial anomalies in combined methylmalonic aciduria and homocystinuria due to a defect in cobalamin metabolism. *Journal of Inherited Metabolic Disease*, *22*(3), 247–250. https://doi.org/10.1023/A:1005521702298

Chen, T., Sui, C., Lin, S., Guo, B., Wang, Y., & Yang, L. (2022). Follow-up study of neuropsychological scores of infant patients with cobalamin C defects and influencing factors of cerebral magnetic resonance imaging characteristics. *Frontiers in Neuroscience*, *16*, 1093850. https://doi.org/10.3389/fnins.2022.1093850

Chern, T., Achilleos, A., Tong, X., Hsu, C.-W., Wong, L., & Poché, R. A. (2020). Mouse models to study the pathophysiology of combined methylmalonic acidemia and homocystinuria, cblC type. *Developmental Biology*, *468*(1–2), 1–13. https://doi.org/10.1016/j.ydbio.2020.09.005

Curpăn, A. S., Balmus, I.-M., Dobrin, R. P., Ciobica, A., Chele, G. E., Gorgan, D. L., & Boloș, A. (2022). A Mini-Review Regarding the Modalities to Study Neurodevelopmental Disorders-Like Impairments in Zebrafish—Focussing on Neurobehavioural and Psychological Responses. *Brain Sciences*, *12*(9), 1147. https://doi.org/10.3390/brainsci12091147

De Abreu, M. S., Genario, R., Giacomini, A. C. V. V., Demin, K. A., Lakstygal, A. M., Amstislavskaya, T. G., Fontana, B. D., Parker, M. O., & Kalueff, A. V. (2020). Zebrafish as a Model of Neurodevelopmental Disorders. *Neuroscience*, *445*, 3–11. https://doi.org/10.1016/j.neuroscience.2019.08.034

Duncan, K. M., Mukherjee, K., Cornell, R. A., & Liao, E. C. (2017). Zebrafish models of orofacial clefts. *Developmental Dynamics*, *246*(11), 897–914. https://doi.org/10.1002/dvdy.24566

Dougnon, G., & Matsui, H. (2022). Modelling Autism Spectrum Disorder (ASD) and Attention-Deficit/Hyperactivity Disorder (ADHD) Using Mice and Zebrafish. *International Journal of Molecular Sciences*, *23*(14), 7550. https://doi.org/10.3390/ijms23147550

Enns, G. M., Barkovich, A. J., Rosenblatt, D. S., Fredrick, D. R., Weisiger, K., Ohnstad, C., & Packman, S. (1999). Progressive neurological deterioration and MRI changes in cblC methylmalonic acidaemia treated with hydroxocobalamin. *Journal of Inherited Metabolic Disease*, *22*(5), 599–607. https://doi.org/10.1023/A:1005517727451

Frattini, D., Fusco, C., Ucchino, V., Tavazzi, B., & Della Giustina, E. (2010). Early Onset Methylmalonic Aciduria and Homocystinuria cblC Type With Demyelinating Neuropathy. *Pediatric Neurology*, *43*(2), 135–138. https://doi.org/10.1016/j.pediatrneurol.2010.04.007

Hannibal, L., & Jacobsen, D. W. (2022). Intracellular processing of vitamin B12 by MMACHC (CblC). In *Vitamins and Hormones* (Vol. 119, pp. 275–298). Elsevier. https://doi.org/10.1016/bs.vh.2022.02.001

Howe, K., Clark, M. D., Torroja, C. F., Torrance, J., Berthelot, C., Muffato, M., Collins, J. E., Humphray, S., McLaren, K., Matthews, L., McLaren, S., Sealy, I., Caccamo, M., Churcher, C., Scott, C., Barrett, J. C., Koch, R., Rauch, G.-J., White, S., … Stemple, D. L. (2013).

The zebrafish reference genome sequence and its relationship to the human genome. *Nature*, *496*(7446), 498–503. https://doi.org/10.1038/nature12111

Kallai, J., Makany, T., Csatho, A., Karadi, K., Horvath, D., Kovacs-Labadi, B., Jarai, R., Nadel, L., & Jacobs, J. W. (2007). Cognitive and affective aspects of thigmotaxis strategy in humans. *Behavioral Neuroscience*, *121*(1), 21–30. https://doi.org/10.1037/0735-7044.121.1.21

Kalueff, A. V., Gebhardt, M., Stewart, A. M., Cachat, J. M., Brimmer, M., Chawla, J. S., Craddock, C., Kyzar, E. J., Roth, A., Landsman, S., Gaikwad, S., Robinson, K., Baatrup, E., Tierney, K., Shamchuk, A., Norton, W., Miller, N., Nicolson, T., Braubach, O., … Schneider, and the Zebrafish Neuros, H. (2013). Towards a Comprehensive Catalog of Zebrafish Behavior 1.0 and Beyond. *Zebrafish*, *10*(1), 70–86. https://doi.org/10.1089/zeb.2012.0861

Kalueff, A. V., & Stewart, A. M. (Eds.). (2012). *Zebrafish Protocols for Neurobehavioral Research* (Vol. 66). Humana Press. https://doi.org/10.1007/978-1-61779-597-8

Kalueff, A. V., Stewart, A. M., & Gerlai, R. (2014). Zebrafish as an emerging model for studying complex brain disorders. *Trends in Pharmacological Sciences*, *35*(2), 63–75. https://doi.org/10.1016/j.tips.2013.12.002

Lee, N., & Kim, D. (2022). Toxic Metabolites and Inborn Errors of Amino Acid Metabolism: What One Informs about the Other. *Metabolites*, *12*(6), 527. https://doi.org/10.3390/metabo12060527

Lerner-Ellis, J. P., Tirone, J. C., Pawelek, P. D., Doré, C., Atkinson, J. L., Watkins, D., Morel, C. F., Fujiwara, T. M., Moras, E., Hosack, A. R., Dunbar, G. V., Antonicka, H., Forgetta, V., Dobson, C. M., Leclerc, D., Gravel, R. A., Shoubridge, E. A., Coulton, J. W., Lepage, P., … Rosenblatt, D. S. (2006). Identification of the gene responsible for methylmalonic

aciduria and homocystinuria, cblC type. *Nature Genetics*, *38*(1), 93–100. https://doi.org/10.1038/ng1683

Li, K., Fan, L., Tian, Y., Lou, S., Li, D., Ma, L., Wang, L., & Pan, Y. (2022). Application of zebrafish in the study of craniomaxillofacial developmental anomalies. *Birth Defects Research*, *114*(12), 583–595. https://doi.org/10.1002/bdr2.2014

Mork, L., & Crump, G. (2015). Zebrafish Craniofacial Development. In *Current Topics in Developmental Biology* (Vol. 115, pp. 235–269). Elsevier. https://doi.org/10.1016/bs.ctdb.2015.07.001

Nguyen, M. G., Tronick, L., Modirian, F., Mardach, R., & Besterman, A. D. (2022). Neurodevelopmental and Neuropsychiatric Disorders in Cobalamin C Disease: A Case Report and Review of the Literature. *Molecular Case Studies*, mcs.a006179. https://doi.org/10.1101/mcs.a006179

Norton, W. H. J. (2013). Toward developmental models of psychiatric disorders in zebrafish. *Frontiers in Neural Circuits*, *7*. https://doi.org/10.3389/fncir.2013.00079

Orger, M. B., & De Polavieja, G. G. (2017). Zebrafish Behavior: Opportunities and Challenges. *Annual Review of Neuroscience*, *40*(1), 125–147. https://doi.org/10.1146/annurev-neuro-071714-033857

Paz, D., Pinales, B. E., Castellanos, B. S., Perez, I., Gil, C. B., Madrigal, L. J., ... & Quintana, A. M. (2023). Abnormal chondrocyte development in a zebrafish model of cblC syndrome restored by an MMACHC cobalamin binding mutant. *Differentiation*, *131*, 74-81.

Quintana, A.M., Geiger, E.A., Achilly, N., Rosenblatt, D.S., Maclean, K.N., Stabler, S.P., Artinger, K.B., Appel, B., Shaikh, T.H., 2014. Hcfc1b, a zebrafish ortholog of HCFC1,

regulates craniofacial development by modulating mmachc expression. Dev. Biol. 396, 94–106. https://doi.org/10.1016/j.ydbio.2014.09.026.

Quintana, A.M., Hernandez, J.A., Gonzalez, C.G., 2017a. Functional analysis of the zebrafish ortholog of HMGCS1 reveals independent functions for cholesterol and isoprenoids in craniofacial development. PLoS One 12, e0180856. https://doi.org/ 10.1371/journal.pone.0180856.

Quintana, A.M., Yu, H.-C., Brebner, A., Pupavac, M., Geiger, E.A., Watson, A., Castro, V. L., Cheung, W., Chen, S.-H., Watkins, D., Pastinen, T., Skovby, F., Appel, B., Rosenblatt, D.S., Shaikh, T.H., 2017b. Mutations in THAP11 cause an inborn error of cobalamin metabolism and developmental abnormalit

Rai, A. R., Joy, T., Rashmi, K. S., Rai, R., Vinodini, N. A., & Jiji, P. J. (2022). Zebrafish as an experimental model for the simulation of neurological and craniofacial disorders. *Veterinary World*, 22–29. https://doi.org/10.14202/vetworld.2022.22-29

Raterman, S. T., Metz, J. R., Wagener, F. A. D. T. G., & Von den Hoff, J. W. (2020). Zebrafish Models of Craniofacial Malformations: Interactions of Environmental Factors. *Frontiers in Cell and Developmental Biology*, *8*, 600926. https://doi.org/10.3389/fcell.2020.600926

Reyes-Nava, N., Yu, H.-C., Coughlin, C. R., Shaikh, T. H., & Quintana, A. M. (2020). Abnormal expression of GABAA receptor sub-units and hypomotility upon loss of *gabra1* in zebrafish. *Biology Open*, bio.051367. https://doi.org/10.1242/bio.051367

Rosenblatt, D. S., Aspler, A. L., Shevell, M. I., Pletcher, B. A., Fenton, W. A., & Seashore, M. R. (1997). Clinical heterogeneity and prognosis in combined methylmalonic aciduria and homocystinuria (cblC). *Journal of Inherited Metabolic Disease*, *20*(4), 528–538. https://doi.org/10.1023/A:1005353530303

Scalais, E., Geron, C., Pierron, C., Cardillo, S., Schlesser, V., Mataigne, F., Borde, P., & Regal, L. (2023). Would, early, versus late hydroxocobalamin dose intensification treatment, prevent cognitive decline, macular degeneration and ocular disease, in 5 patients with early-onset cblC deficiency? *Molecular Genetics and Metabolism*, *140*(3), 107681. https://doi.org/10.1016/j.ymgme.2023.107681

Schindelin, J., Arganda-Carreras, I., Frise, E., Kaynig, V., Longair, M., Pietzsch, T., Preibisch, S., Rueden, C., Saalfeld, S., Schmid, B., Tinevez, J.-Y., White, D. J., Hartenstein, V., Eliceiri, K., Tomancak, P., & Cardona, A. (2012). Fiji: An open-source platform for biological-image analysis. *Nature Methods*, *9*(7), 676–682. https://doi.org/10.1038/nmeth.2019

Sloan, J. L., Achilly, N. P., Arnold, M. L., Catlett, J. L., Blake, T., Bishop, K., Jones, M., Harper, U., English, M. A., Anderson, S., Trivedi, N. S., Elkahloun, A., Hoffmann, V., Brooks, B. P., Sood, R., & Venditti, C. P. (2020). The vitamin B12 processing enzyme, mmachc, is essential for zebrafish survival, growth and retinal morphology. *Human Molecular Genetics*, *29*(13), 2109–2123. https://doi.org/10.1093/hmg/ddaa044

Stewart, A. M., Braubach, O., Spitsbergen, J., Gerlai, R., & Kalueff, A. V. (2014). Zebrafish models for translational neuroscience research: From tank to bedside. *Trends in Neurosciences*, *37*(5), 264–278. https://doi.org/10.1016/j.tins.2014.02.011

Tegelenbosch, R. A. J., Noldus, L. P. J. J., Richardson, M. K., & Ahmad, F. (2012). Zebrafish embryos and larvae in behavioural assays. *Behaviour*, *149*(10–12), 1241–1281. https://doi.org/10.1163/1568539X-00003020

Trefz, F. K., Scheible, D., Frauendienst-Egger, G., Huemer, M., Suomala, T., Fowler, B., Haas, D., & Baumgartner, M. R. (2016). Successful intrauterine treatment of a patient with

cobalamin C defect. *Molecular Genetics and Metabolism Reports*, *6*, 55–59. https://doi.org/10.1016/j.ymgmr.2016.01.005

Weisfeld-Adams, J. D., Bender, H. A., Miley-Åkerstedt, A., Frempong, T., Schrager, N. L., Patel, K., Naidich, T. P., Stein, V., Spat, J., Towns, S., Wasserstein, M. P., Peter, I., Frank, Y., & Diaz, G. A. (2013). Neurologic and neurodevelopmental phenotypes in young children with early-treated combined methylmalonic acidemia and homocystinuria, cobalamin C type. *Molecular Genetics and Metabolism*, *110*(3), 241–247. https://doi.org/10.1016/j.ymgme.2013.07.018

Van De Burgt, N., Van Doesum, W., Grevink, M., Van Niele, S., De Koning, T., Leibold, N., Martinez-Martinez, P., Van Amelsvoort, T., & Cath, D. (2023). Psychiatric manifestations of inborn errors of metabolism: A systematic review. *Neuroscience & Biobehavioral Reviews*, *144*, 104970. https://doi.org/10.1016/j.neubiorev.2022.104970

Vaz, R., Hofmeister, W., & Lindstrand, A. (2019). Zebrafish Models of Neurodevelopmental Disorders: Limitations and Benefits of Current Tools and Techniques. *International Journal of Molecular Sciences*, *20*(6), 1296. https://doi.org/10.3390/ijms20061296

## Curriculum Vitae

Briana E. Pinales, Bachelor's of Science from the University of Texas at El Paso with a minor in Psychology and doctorate of Biological Sciences from the University of Texas at El Paso. Research experiences included the mentorship under Dr. Anita M Quintana at the Department of Biological sciences. Experience working there included learning mentoring, poster presentations, Behavioral testing, and data analysis using image J software. investigating congenital anomalies using the zebrafish model organism to study behavior and craniofacial malformation. Current publications the titles: Abnormal chondrocyte development in a zebrafish model of cblC syndrome restored by an MMACHC cobalamin binding mutant. Differentiation, 131, 74–81. https://doi.org/10.1016/j.diff.2023.04.003, Overexpression of MMACHC Prevents Craniofacial Phenotypes Caused by Knockdown of znf143b. American Journal of Undergraduate Research, 20(1), 77–84. https://doi.org/10.33697/ajur.2023.081, Overexpression of corticotropin-releasing factor in the nucleus accumbens enhances the reinforcing effects of nicotine in intact female versus male and ovariectomized female rats. Neuropsychopharmacology: official publication of the American College of Neuropsychopharmacology, 45(2), 394–403. https://doi.org/10.1038/s41386-019-0543-0 and a open access textbook chapter. Chapter 5: Early brain development and environmental influence. Open Access Textbook. Introduction to behavioral neuroscience. Openstax. Eds. Elizabeth Kirby, Melissa Glen, Christina Williams, and Noah Sandstrom. Under revision.

Email for contact: brianaepinales@gmail.com